Mathematisches Forschungsinstitut Oberwolfach

Mechanics of Materials: Mechanics of Interfaces and Evolving Microstructure

Organised by
Reinhold Kienzler, Bremen
David L. McDowell, Atlanta
Stefan Müller, Bonn
Ewald A. Werner, München

13 March – 19 March 2016

ABSTRACT. Emphasis in modern day efforts in mechanics of materials is increasingly directed towards integration with computational materials science, which itself rests on solid physical and mathematical foundations in thermodynamics and kinetics of processes. Practical applications demand attention to length and time scales which are sufficiently large to preclude direct application of quantum mechanics approaches; accordingly, there are numerous pathways to mathematical modelling of the complexity of material structure during processing and in service. The conventional mathematical machinery of energy minimization provides guidance but has limited direct applicability to material systems evolving away from equilibrium. Material response depends on driving forces, whether arising from mechanical, electromagnetic, or thermal fields. When microstructures evolve, as during plastic deformation, progressive damage and fracture, corrosion, stress-assisted diffusion, migration or chemical/thermal aging, the associated classical mathematical frameworks are often ad hoc and heuristic. Advancing new and improved methods is a major focus of 21st century mechanics of materials of interfaces and evolving microstructure.

Introduction by the Organisers

The workshop *Mechanics of Materials: Mechanics of Interfaces and Evolving Microstructure* attracted about 50 participants with broad geographic representation from Europe and the United States. This workshop was a well balanced blend of researchers with backgrounds in mathematics, mechanics and materials science.

The organizers successfully recruited a significant number of younger representatives of the mentioned research communities.

One of the most pressing current trends in materials discovery, design and development involves the intersection of applied mathematics and computational/data sciences with mechanics of materials and computational materials science to enhance understanding and to produce improved next generation computational methods and materials modelling tools. This places increased emphasis on the predictive nature of computational mechanics pertaining to realistic material nanostructures and microstructures. Material complexity is high - today's leading materials are hierarchical, having characteristics of structure at multiple length scales to satisfy a complex set of performance requirements and constraints. This is true for materials in electronic devices, in automotive and aerospace applications, multilayers for electronics and MEMS applications, interfaces for catalysis and chemical separations, and numerous application domains.

This state of affairs motivated the central theme of this workshop, namely to explore new and emerging mathematical approaches to describe interface properties and to quantify evolving microstructures. Owing to the mutual dependence of properties on various scales, improved methods (both physically and mathematically based) must be developed to describe correctly equilibrium and non-equilibrium microstructure evolution at multiple length scales and time scales. There are serious unresolved physical and mathematical issues in applying phase field theory to realistic microstructures, up-scaling atomistic simulations to relevant time and length scales, how to address the complexity of potential energy landscapes that govern interface structure and microstructure rearrangements in materials undergoing deformation, damage, and phase/structure transitions, mathematical methods to manage complexity of many body structure and defect fields in real materials (big data and inverse modelling/data analytics), and mathematical approaches to representing grain boundary and phase interfaces in materials with an eye towards field theories that facilitate up-scaling.

Based on the above outline of current and highly relevant topics and the experience gained in organizing preceding workshops on mechanics of materials, the following main topics were suggested:

- Phase field modeling and relations to realistic microstructures at multiple scales, as well as other approaches to similar field equations.
- Coarse graining atomistic simulations to longer length and time scales to support materials development.
- Mathematical methods for convergence in homogenization of materials with microstructure (e.g., Γ-convergence).
- Thermodynamics and kinetics of evolving microstructure, including novel mathematical approaches to explore complex energy landscapes of interfaces and heterostructures.
- Methods for reducing the order of continuum descriptions and mathematical techniques and data sciences approaches to address the "big data"

> aspect of complex hierarchy of material structure and its relation to properties.

- Mathematical representation of evolving interfaces to facilitate field theory approaches that bridge with atomistic and continuum levels of treatment.

The sequence and duration of the sessions were defined on Monday morning. They were moderated by session chairs and each consisted of 1-2 overview lectures (30-40 minutes each, including discussion), along with several short "thought piece" contributions (2-3 presentations, each 15 minutes). Ample time was devoted to discussion, both during and following presentations. The format of sessions (subject to hard stops for lunch and dinner), including coffee breaks, gave the flexibility to maximize productive discussion. Reports from the session chairs were summarized and discussed extensively on Friday.

The organizers regard this particular workshop as among the most successful in the topical area of Mechanics of Materials in recent memory, for several reasons. First, a number of young participants were involved and highly active in presentations and discussions, representing the next generation of blending applied mathematics with mechanics of materials. Second, the discussions were detailed and animated from the outset, with many useful points and counterpoints discussed. We believe that this workshop has launched many potentially fruitful couplings of researchers in Europe and the USA, and has defined some specific target areas as goals for mathematics, including extended methods that can consider convergence characteristic of homogenization methods for evolving microstructure, include viscoplastic, dissipative cases, extreme value properties/responses in addition to mean responses, methods for constrained optimization of nonconvex energy potentials with relevance to shear banding and formation of laminate microstructures, and enhancement of mathematical approaches for modelling the role interfaces.

Workshop: Mechanics of Materials: Mechanics of Interfaces and Evolving Microstructure

Table of Contents

Abstracts

Numerical solution of generalized mechanics based on a variational formulation

B. EMEK ABALI

(joint work with Wolfgang H. Müller)

A beam of a length in micrometer range shows a phenomenon called *size effect* that is well-observed in experiments. Classical mechanics fails to describe this phenomenon accurately. Various proposals in the literature are called with different names, viz., strain gradient theory, micropolar theory, micromorphic theory. They all have higher gradients in space, which play a role in the formulation of the theory. For the case of elasticity we present the variational formulation including second gradients in space and obtain the weak form necessary for performing numerical simulations.

1. PRINCIPLE OF LEAST ACTION IN GENERALIZED MECHANICS

In order to obtain the weak form there are different possible approaches used in the literature. A usual way is to start with balance equations and determine the field equations describing the system. In case of classical mechanics, where we ignore electric charge and any deviation from the reference temperature, we employ the balance of linear momentum in order to calculate displacements. In this approach the balance of linear momentum is the axiom; we just start with it.

Another approach is to start axiomatically with a LAGRANGEan density, $\mathcal{L}$. For example, in case of classical mechanics,

$$(1) \qquad \mathcal{L} = \mathcal{L}\big(x_\mu, \phi_A, \phi_{A,\mu}\big) \ ,$$

states that there is a function capable of describing the system. This LAGRANGEan density depends on any number of coordinates, x_μ, on some primitive variables, ϕ_A, and on its first gradients, $\phi_{A,\mu}$. The generalization is now obvious: In case of generalized mechanics we include at least one more gradient of the primitive variables such that LAGRANGEan density in generalized mechanics becomes

$$(2) \qquad \mathcal{L} = \mathcal{L}\big(x_\mu, \phi_A, \phi_{A,\mu}, \phi_{A,\mu\nu}\big) \ .$$

For orthonormal coordinates we can introduce an action functional:

$$(3) \qquad \mathcal{A} = \int_\Omega \mathcal{L} \, \mathrm{d}\Sigma \ , \quad \mathrm{d}\Sigma = \mathrm{d}x_1 \, \mathrm{d}x_2 \ldots \mathrm{d}x_m \ .$$

The principle of least action asserts that this action is an invariant under a transformation of primitive variables and its derivatives. In other words, the value of action

remains the same if we apply an arbitrary transformation in $\{\phi_A, \phi_{A,\mu}, \phi_{A,\mu\nu}\}$ as $\{\phi'_A, \phi'_{A,\mu}, \phi'_{A,\mu\nu}\}$ such that

$$\delta\mathcal{A} = 0 \ ,$$

(4)
$$\delta\mathcal{A} = \int_\Omega \mathcal{L}' \, \mathrm{d}\Sigma - \int_\Omega \mathcal{L} \, \mathrm{d}\Sigma \ .$$

The prime of LAGRANGEan density has the following meaning:

$$\mathcal{L}' = \mathcal{L}\big(x_\mu, \phi'_A, \phi'_{A,\mu}, \phi'_{A,\mu\nu}\big) \ ,$$

(5)
$$\phi'_A = \phi_A + \varepsilon\delta\phi_A \ , \quad \phi'_{A,\mu} = \phi_{A,\mu} + \varepsilon\delta\phi_{A,\mu} \ , \quad \phi'_{A,\mu\nu} = \phi_{A,\mu\nu} + \varepsilon\delta\phi_{A,\mu\nu} \ ,$$

with a small number ε the so-called *test* functions, $\delta\phi_A$, are arbitrary. We can now expand $\mathcal{L}'$,

(6)
$$\mathcal{L}' = \mathcal{L} + \frac{\partial\mathcal{L}}{\partial\phi_A}\varepsilon\delta\phi_A + \frac{\partial\mathcal{L}}{\partial\phi_{A,\mu}}\varepsilon\delta\phi_{A,\mu} + \frac{\partial\mathcal{L}}{\partial\phi_{A,\mu\nu}}\varepsilon\delta\phi_{A,\mu\nu} \ ,$$

and obtain out of the principle of least action by dividing by the constant ε,

(7)
$$\int_\Omega \left(\frac{\partial\mathcal{L}}{\partial\phi_A}\delta\phi_A + \frac{\partial\mathcal{L}}{\partial\phi_{A,\mu}}\delta\phi_{A,\mu} + \frac{\partial\mathcal{L}}{\partial\phi_{A,\mu\nu}}\delta\phi_{A,\mu\nu} \right) \mathrm{d}\Sigma = 0 \ .$$

The coordinates are space, $X_i \in \mathcal{B}_0$, denoting to particles; and time, $t \in \tau$, such that the latter variational form reads

(8)
$$\int_\tau \int_{\mathcal{B}_0} \left(\frac{\partial\mathcal{L}}{\partial\phi_A}\delta\phi_A + \frac{\partial\mathcal{L}}{\partial\dot\phi_A}\delta\dot\phi_A + \frac{\partial\mathcal{L}}{\partial\phi_{A,i}}\delta\phi_{A,i} + \right.$$
$$\left. + \frac{\partial\mathcal{L}}{\partial\ddot\phi_A}\delta\ddot\phi_A + \frac{\partial\mathcal{L}}{\partial\dot\phi_{A,i}}\delta\dot\phi_{A,i} + \frac{\partial\mathcal{L}}{\partial\phi_{A,ij}}\delta\phi_{A,ij} \right) \mathrm{d}V \, \mathrm{d}t = 0 \ .$$

Furthermore, for addressing boundary terms we need the redefine the action functional:

(9)
$$\mathcal{A} = \int_\tau \int_{\mathcal{B}_0} \mathcal{L} \, \mathrm{d}V \, \mathrm{d}t + \int_\tau \int_{\partial\mathcal{B}_0} W_\mathrm{s} \, \mathrm{d}A \, \mathrm{d}t + \int_\tau \int_{\partial\partial\mathcal{B}_0} W_\mathrm{e} \, \mathrm{d}\ell \, \mathrm{d}t,$$

since we have second gradients in primitive variables, $\partial\partial\mathcal{B}_0$ is admissible, where $\mathrm{d}\ell$ denotes a line element. We assume that W_s and W_e depend only on primitive variables in order to have a physical interpretation of the boundary terms.

2. Generating the weak form

For a numerical calculation such as by using finite element method, we necessitate the weak form following naturally from Eq. (8) after integrating by parts all the terms with a time rate in the test functions,

(10)
$$\int_{\mathcal{B}_0} \left(\frac{\partial\mathcal{L}}{\partial\phi_A}\delta\phi_A - \left(\frac{\partial\mathcal{L}}{\partial\dot\phi_A}\right)^{\!\cdot}\delta\phi_A + \frac{\partial\mathcal{L}}{\partial\phi_{A,i}}\delta\phi_{A,i} + \right.$$
$$\left. + \left(\frac{\partial\mathcal{L}}{\partial\ddot\phi_A}\right)^{\!\cdot\cdot}\delta\phi_A - \left(\frac{\partial\mathcal{L}}{\partial\phi_{A,i}}\right)^{\!\cdot\cdot}\delta\phi_{A,i} + \frac{\partial\mathcal{L}}{\partial\phi_{A,ij}}\delta\phi_{A,ij} \right) \mathrm{d}V +$$
$$+ \int_{\partial\mathcal{B}_0} \frac{\partial W_\mathrm{s}}{\partial\phi_A}\delta\phi_A \, \mathrm{d}A + \int_{\partial\partial\mathcal{B}_0} \frac{\partial W_\mathrm{e}}{\partial\phi_A}\delta\phi_A \, \mathrm{d}\ell \ ,$$

where the boundary (in time) terms vanish. This fact can be seen as prescribing ϕ_A and $\phi_A^{\bullet}$ in the initial time, we know the values in the last two time steps by considering in a discrete in time fashion. Since we know the values the test function vanishes on the (time) boundaries. The latter integral form in Eq. (10) is called the *weak form*.

In mechanics the only primitive variable is the displacement:

$$(11) \qquad\qquad \phi_A = u_i \ , \quad u_i = x_i - X_i \ ,$$

which indicates the difference between the current position, x_i, and the reference position, X_i, denoting the particles. For the LAGRANGEan energy density we can employ the following function:

$$(12) \qquad\qquad \mathcal{L} = \frac{1}{2}\rho_0 u_i^{\bullet} u_i^{\bullet} - w + \rho_0(f_i u_i + l_{ij} u_{j,i}) \ ,$$

where the first term addresses the kinetic energy density, w is the stored energy density, the last term creates volumetric change in the displacement and its gradient. For the energy densities on the boundaries we may choose a simple approach: The energy density on the surface, $W_{\mathrm{s}} = \hat{t}_i u_i$, gets use of a traction vector, $\hat{t}_i$, as the force per area; since a physical interpretation is difficult we may set the energy on the line as being zero, $W_{\mathrm{e}} = 0$. Now by inserting the energies on the boundary and lines into the weak form and after using EULER backwards time discretization with a finite element method in space, the weak form for generalized mechanics reads

(13)

$$\mathrm{Form} = \sum_{n=1}^{\mathrm{ele.}} \int_{E^n} \left(\rho_0 f_i \delta u_i - \rho_0 \frac{u_i - 2u_i^0 + u_i^{00}}{\Delta t \Delta t} \delta u_i - \frac{\partial w}{\partial u_{i,j}} \delta u_{i,j} + \rho_0 l_{ji} \delta u_{i,j} - \right.$$

$$\left. -\frac{1}{\Delta t \Delta t}\left(\frac{\partial w}{\partial u_{i,j}} - 2\frac{\partial w^0}{\partial u_{i,j}^0} + \frac{\partial w^{00}}{\partial u_{i,j}^{00}} \right) \delta u_{i,j} - \frac{\partial w}{\partial u_{i,jk}} \delta u_{i,jk} \right) \mathrm{d}V + \int_{\partial \mathcal{B}_0} \hat{t}_i \delta u_i \, \mathrm{d}A \ ,$$

with

$$(14) \qquad \begin{aligned} w^0 &= w(E_{ij}^0, E_{ij,k}^0) \ , \quad w^{00} = w(E_{ij}^{00}, E_{ij,k}^{00}) \ , \\ E_{ij}^0 &= \frac{1}{2}u_{k,i}^0 u_{k,j}^0 + u_{(i,j)}^0 \ , \quad E_{ij}^{00} = \frac{1}{2}u_{k,i}^{00} u_{k,j}^{00} + u_{(i,j)}^{00} \ . \end{aligned}$$

For a successful implementation we only need an adequate definition of the stored energy density. Depending on this energy definition one can construct different theories existing in the literature. The simplest choice is quadratic in strain and strain gradients:

$$(15) \quad w = w(E_{ij}, E_{ij,k}) = E_{ij} C_{ijkl} E_{kl} + E_{ij,k} D_{ijklmn} E_{lm,n} + E_{ij} G_{ijklm} E_{kl,m} \ ,$$

for a homogeneous material, where the strain can be a nonlinear measure:

$$(16) \qquad\qquad E_{ij} = \frac{1}{2}u_{k,i}u_{k,j} + u_{(i,j)} \ .$$

We refer to [1] or [2] for a concrete representation of the coefficients, C_{ijkl}, D_{ijklmn}, G_{ijklm}, for isotropic materials.

By using the weak form in Eq. (13) we can implement and solve any particular problem with strain gradient elasticity. We recall that the weak form has been taken out from a variational formulation. This formulation seems to be more beneficial for a generalization since the only way to generalize the LAGRANGEan density relies on adding one more gradients of primitive variables.

REFERENCES

[1] F. dell'Isola, G. Sciarra, S. Vidoli, *Generalized Hooke's law for isotropic second gradient materials*, Proceedings of the Royal Society A: Mathematical, Physical and Engineering Science, **465** (2009), 2177–2196.
[2] B. E. Abali, W. H. Müller, V. A. Eremeyev, *Strain gradient elasticity with geometric non-linearities and its computational evaluation*, Mechanics of Advanced Materials and Modern Processes, **1**(1) (2015), 1–11.

Calculation of stress field of a disconnection

AMIT ACHARYA

(joint work with Chiqun Zhang)

We demonstrate a method for mathematically representing a disconnection defect in a grain boundary

  (1) as a composite of a disclination dipole and a slip dislocation and
  (2) by a dislocation whose Burgers vector is the sum of the effective Burgers vector of the disclination dipole and the slip dislocation.

We then compute the stress and energy density fields of these two configurations and compare them. The calculations are done by a finite element implementation of a novel theory of combined dislocations and generalized disclination defects [1].

REFERENCES

[1] A. Acharya, C. Fressengeas, *Continuum mechanics of the interaction of phase boundaries and dislocations in solids*, G.-Q.G. Chen et al. (eds.), Differential Geometry and Continuum Mechanics, Springer Proceedings in Mathematics and Statistics, **137** (2015), 123–164.

Line defect dynamics and solid mechanics

AMIT ACHARYA

(joint work with Chiqun Zhang, Xiaohan Zhang)

We describe a model of dislocation dynamics in a Pde-setting capable of representing motion of individual dislocations in the presence of inertia and finite deformation effects. We compare our results with molecular dynamic simulations showing supersonic dislocation motion. Our careful computations show an apparent Peierls stress effect in a translationally-invariant Pde-model that demands analytical substantiation or falsification. We also demonstrate calculations of coupled dislocation and disclination fields representing penta-twin configurations observed in nano-crystalline materials (wires).

References

[1] A. Acharya, C. Fressengeas, *Continuum mechanics of the interaction of phase boundaries and dislocations in solids*, G.-Q.G. Chen et al. (eds.), Differential Geometry and Continuum Mechanics, Springer Proceedings in Mathematics and Statistics, **137** (2015), 123–164.

[2] X. Zhang, A. Acharya, N. J. Walkington, J. Bielak, *A single theory for some quasi-static, supersonic, atomic, and tectonic scale applications of dislocations*, Journal of the Mechanics and Physics of Solids, **84** (2015), 145–195.

Balance laws for gradient materials

Albrecht Bertram

Since certain material effects cannot be described within the scope of simple materials - in principle, there has been some interest during recent years in the development of generalized continuum theories like polar-media, micromorphic, and non-local ones. Particularly, gradient materials have been studied, which offer interesting possibilities for modeling and simulation. In these cases, the set of the classical kinematical and dynamic variables that appear in the constitutive equations, is enlarged by higher strain gradients and work-conjugate higher stress tensors. In doing so, a set of interesting questions arises immediately like, e.g.

- How do the balance laws look like?
- What additional boundary conditions are needed?
- What are the properties of the higher-order stress tensors?

Nowadays the usual way to investigate these problems is based on the Principle of Virtual Power (Germain (1972), Bertram (1983), Trostel (1985), Del Piero (2009), and many others). In the present context, the starting point is the power functional. As a Principle of Determinism the existence of a power functional is assumed, which gives the value of the current total power depending on the motion of the body with respect to an observer. Secondly, it is assumed that the power is an objective quantity for admissible motions. As a second step, the power functional is extended on the set of virtual velocity fields in a continuous and linear way, which gives the Principle of Virtual Power (PVP). With this at hand, we can define forces and torques and derive the two balance laws for the linear momentum and moment of momentum. A field formulation of the PVP and the dynamical variables can then be obtained by applying the Riesz representation theorem for linear and continuous functionals. This way, higher-order stress fields are introduced. Their properties can then be studied. By repeatedly applying integration by parts, we obtain the surface terms for the dynamical quantities, from which we can derive the Neumann boundary conditions. However, these become rather lengthy and complicated for higher orders gradient materials. It turns out that all higher-order stress tensors are objective under change of observers. However, only the classical second-order stress tensor is symmetric due to the balance of moment of momentum, while the higher-order ones can only be submitted under the same subsymmetries as the work conjugate kinematical quantities. The order of such gradient theories depends on the Sobolev norm which we introduce on the

set of virtual velocity fields. If the order of it is two, we obtain the classical simple material after Cauchy. The orders higher than two stand for gradient materials. It is interesting that also the order of one gives a reasonable theory. It can be interpreted as a Newton theory for remote masses interacting exclusively by central forces. Here the balance of torques becomes trivial, while the balance of forces remains non-trivial.

A summary of the results and further material modeling of gradient materials can be found under http://www.ifme.ovgu.de/ifme_media/CompendiumGradient-MaterialsJan2016.pdf.

Slip Transfer Geometry and Deformation Anisotropy
Thomas R. Bieler
(joint work with Scott C. Sutton, Bret E. Dunlap, M.A. Crimp, B.L. Boyce)

Heterogeneous deformation is commonly understood as the origin of plastic instabilities that precede damage, so modeling how grain boundaries influence deformation presents an ongoing challenge for mesoscale models. An example is provided (based upon a more extensive discussion in [1, 2]) to illustrate how a simple description of the geometry of slip transfer may or may not be able to provide a means to introduce an appropriate barrier for slip across grain boundaries into a model. A geometric description of slip transfer is illustrated in Fig. 1, showing slip planes and slip directions within grains on either side of a grain boundary. Three angles define the geometry, the angle between the two plane normal directions, the angle between the two slip directions, and the angle that the two planes make in the grain boundary plane. Two commonly used measures of slip transmissibility are the m' parameter introduced by Luster and Morris [3], and a similar parameter identified by Lee, Robertson and Birnbaum [4]. As the angles become smaller, the ease of slip transfer increases. The number of values for these parameters for a given boundary is the number of slip systems squared, but only the values related to active slip systems are relevant. This parameter carries no information about grain boundary energy or its evolution due absorption of dislocations or other defects.

The role of grain boundaries on heterogeneous deformation in an initially polished polycrystalline tantalum polycrystal was examined using EBSP maps obtained after incremental deformation in bending of pure Ta to identify regions of heterogeneous deformation. Figure 2 illustrates an example of slip transfer across a boundary in the center the image after deformation to a strain of $\sim 8\%$. The boundaries above and below do not show slip transfer, and instead, topographic ledges along the boundary suggest that sliding occurred.

Figure 3 gives an example of a slip transfer computation. First, the Schmid factors are computed for all slip systems in grains 86 and 97; <111> slip directions on {110} planes are numbered 1:12, and 13:24 are on {112} planes. The slip systems are sorted in decreasing order of the Schmid factor. For grain 97, {112} slip on system 16 has the highest Schmid factor of 0.47, and the next highest
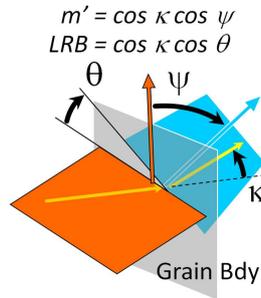
FIGURE 1. Geometry of slip transfer at a grain boundary
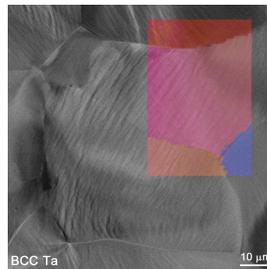
FIGURE 2. Example of grain boundaries in a pre-polished pure Ta sample with observed slip transfer in the middle grain boundary, and lack of slip transfer in boundaries at the top and bottom of the figure. The color overlay indicates grain orientations based upon a normal direction inverse pole figure map.

systems go across the top of the table. Similarly, slip systems in grain 86 are listed downward. The m' parameter is shown within the table for each pair of slip systems. Most of the m' values are rather small in this example, but five in bold font have values above 0.7. Slip systems with higher m' values are illustrated within the unit cells, and the m' values are indicated between the illustrated slip systems. The highest value of m' is 0.93 between the 4th highest slip system in grain 97 with a Schmid factor of 0.45, and the 2nd highest slip system in grain 86 with a Schmid factor of 0.47. Because the actual local stress state is not known at the boundary, and because the local grain orientation along the boundary varies due to orientation gradients resulting from the accumulated deformation, the values are estimates. As a meaningful value of m' for a given boundary is desirable, the highest three values of m' among the most favored four slip systems in each grain are averaged (there are certainly other ways to obtain a meaningful value).

Two rolled and recrystallized specimens are compared, one bent transverse to the original rolling direction, and the other parallel to the rolling direction. Local average misorientation maps are shown in Fig. 4, indicating that some boundaries

slpsys#/Schm   *m'* value table

GB 86-97	16/0.47	6/0.47	22/0.45	12/0.45	5/0.36
7/0.49	0.08	0.02	0.39	0.18	0.13
23/0.47	0.09	0.04	0.79	0.93	0.20
10/0.45	0.03	0.21	0.43	0.77	0.16
20/0.45	0.01	0.03	0.58	0.43	0.02
21/0.40	0.15	0.06	0.09	0.12	0.20
6/0.40	0.74	0.75	0.01	0.01	0.52

1:12 {110} 13:24 {112}

Grain 86
m = 0.47
m = 0.45
0.785
0.931
0.774
m′
m = 0.45
m = 0.45
Tensile Axis
Grain 97
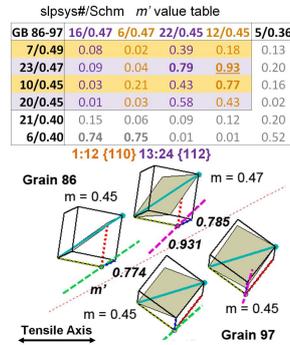
FIGURE 3. Slip transfer calculation between grains 86 and 97 based upon uniaxial tension and average grain orientations in BCC Ta with <111> slip on {110} and {112} planes.

exhibit large orientation gradients close to $2°$, while other boundaries show no misorientation different from that of the grains on either side. The overall pattern of misorientation shows a fairly homogeneous value in the TD sample of about $0.5°$ (light green), while the sample deformed in the rolling direction has much lower orientation gradients within grains, and fewer boundaries with high local average misorientation.

The hypothesis that boundaries with higher orientation gradients may be the result of low m' values was assessed, i.e. a higher density of geometrically necessary dislocations may indicate a dislocation pileup arrangement resulting from the inability to accomplish slip transfer. A reconstructed boundary file (providing segments of grain boundaries with the average grain orientations on either side) was used to compute m', and the value is used to color the boundary according to a color scale illustrated on the horizontal m' axis of the plots in the center of the figure. Then, along each boundary, an estimated value for the misorientation was assigned to the corresponding m' value, and a cumulative distribution was was generated (black dotted lines). Sub populations based upon misorientation bins are indicated by colored lines correlated to the LAM plots. At a cumulative probability of 0.75, the spread between boundaries with low misorientation and high misorientation is the largest in the TD sample (Fig. 4a), indicating that low m' values are correlated with high LAM values, and high m' values with low LAM values for the specimen deformed in the transverse direction (note examples in solid ellipses, and one of many exceptions to the trend noted by the dashed ellipse). However, there is no such correlation for the sample deformed in the rolling direction (Fig. 4b).

This result clearly indicates that the nature of slip as well as slip transfer is distinctly different in the same material deformed in the transverse vs. rolling directions, for reasons that are not clear. The lesser amount of local average misorientation in the sample deformed in the rolling direction may reflect stability
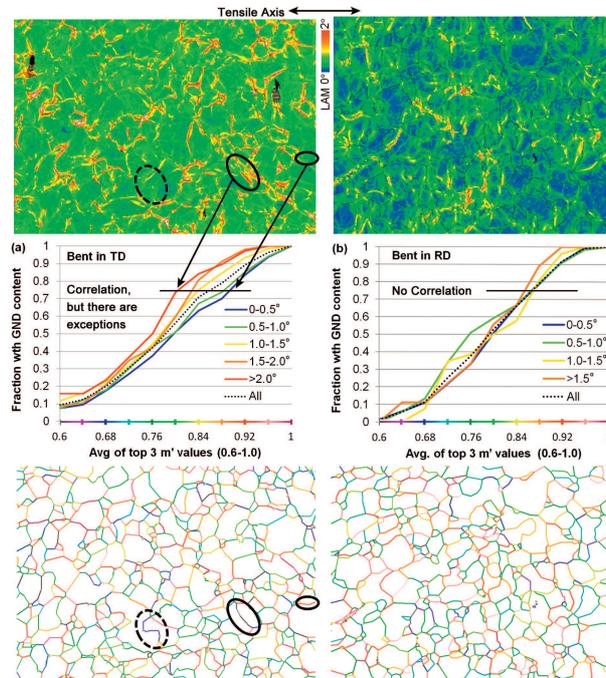
FIGURE 4. Local average misorientation (a measure of geometrically necessary dislocation density) is plotted spatially and compared with average m' values on each boundary in a cumulative distribution plot that indicates a meaningful correlation for the sample deformed in the transverse direction, but not in the rolling direction (Boundaries with m' values less than 0.6 were lumped into a single bin, and are not plotted).

in the grain orientations resulting from the rolling deformation texture and subsequent recrystallization. Such stability may account for fewer grain orientation pairs that deform heterogeneously, which is supported by the different changes in textures shown in Fig. 5, where strengthening of texture occurred in both samples. The strengthening was less in the transverse deformation, leading to a four-fold symmetric set of orientations, suggesting that many grain orientations were less stable, and rotated, leading to a more varied range of dislocation activity.

There are clearly improvements that can be made in such an analysis. First, comparison of observed slip bands with favored slip systems will indicate which slip systems are most active, and lead to better guidance on choosing what values of m' are most meaningful for the boundary. Second, evaluation of m' along the boundary using local orientations will lead to varying measures of m' with position, which can be more directly compared to observable features related to ledge formation and slip transfer. This may lead to identification of a m' threshold value
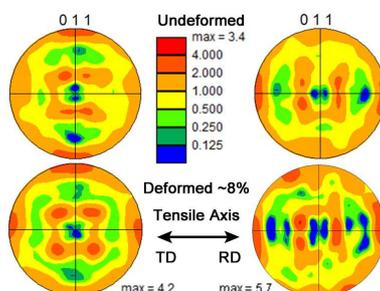
FIGURE 5. The texture changes in the transverse and rolling directions are illustrated in (011) pole figures. In both cases the texture sharpened, but there was more reorientation in the transverse direction.

below which slip transfer is not likely. Ideally, comparison with a geometrically accurate computational model of the same microstructure would enable the local stress tensor as well as the amount of shear to be identified, and this could be used as a way to identify which slip systems are most favored, and to examine whether m' or similar parameters can account for observed heterogeneous features. Such an approach is illustrated in [1] for a titanium alloy microstructural patch where such ideas are examined in greater detail. However, it is not clear if any of these refinements could result in a meaningful predictor of slip transmission in the rolling direction deformation.

REFERENCES

[1] T. R. Bieler, P. Eisenlohr, C. Zhang, H. Phukan, M. A. Crimp, *Grain boundaries and interfaces in slip transfer*, Current Opinion in Solid State and Materials Science, **18**(4) (2014), 212–226.
[2] T. R. Bieler, S. C. Sutton, B. E. Dunlap, Z. A. Keith, P. Eisenlohr, M. A. Crimp, B. L. Boyce, *Grain Boundary Responses to Heterogeneous Deformation in Tantalum Polycrystals*, JOM **66**(1) (2014), 121–128.
[3] J. Luster, M. A. Morris, *Compatibility of deformation in two-phase Ti-Al alloys: dependence on microstructure and orientation relationships*, Metall. Mater. Trans. A **26** (1995), 1745–1756.
[4] T. C. Lee, J. M. Robertson, H. K. Birnbaum, *Prediction of slip transfer mechanisms across grain boundaries*, Scripta Metallurgica **23**(5) (1989), 799–803.

The Method of CAC: A Concurrent Atomistic-Continuum Methodology

YOUPING CHEN

(joint work with David L. McDowell)

This talk starts with an overview of coarse grained atomistic methods and major challenges in the developments of general static and dynamic concurrent multiscale methods, i.e., the existence of ghost force, the spurious wave reflection and the defect reflection by numerical interfaces that link regions governed by different materials descriptions. We assert that the origin of the problems is the mismatch of the materials descriptions, which gives rise to the mismatch of phonon representation and defect representation. We argue that, to develop a concurrent atomistic-continuum method for dynamic simulation, we must unify the formulations of their governing laws; for this unified formulation, we must go beyond the existing statistical mechanics methods to develop a new formalism; this new formulism should lead to reformulation of continuum mechanics to include the information of molecular structure and interaction and to recast of the governing equation to facilitate simulation of discontinuous phenomena.

We then introduce a new formalism, with which a crystalline material is described as a continuous collection of material points (or lattice cells), while embedded within each material point is a group of discrete atoms. Following the nonequilibrium statistical mechanical theory of transport processes developed by Irving-Kirkwood, this concurrent two-level description leads to a new multiscale mathematical representation of the balance law, as exact consequences of Newton's second law. The new balance equations, supplemented by the underlying interatomic potential, solve for both the continuous lattice deformation and the rearrangement of atoms within the lattice cells, naturally resulting in a concurrent atomistic-continuum methodology (CAC); the two limiting cases, i.e., the atomic and the macroscopic scales, recover the atomistic and continuum descriptions of transport processes, respectively. The resulted single set of balance equations govern both static and dynamic problems, thermo-mechanical and thermal transport problems, and monatomic and polyatomic materials. Numerical examples of the CAC simulation are briefly presented, including CA simulation of the fast moving dislocations and the comparison between CAC and MD results, the propagation of heat pulse in single crystalline materials, and the dynamic interaction between phonons and dislocations and that between phonons and grain boundaries.

Dislocation models of semicoherent interfaces

MICHAEL DEMKOWICZ

Semicoherent interfaces between crystalline solids are interfaces whose internal, in-plane structure may be described as a network of dislocations. The regions between the dislocations are coherent, i.e. they are characterized by perfect, atom-to-atom matching of the neighboring crystals. The dislocations that separate these regions

accommodate differences in lattice parameter, crystal structure, or orientation between the neighboring crystals. Much work has recently been devoted to modeling semicoherent interfaces and their properties [1].

The structure of semicoherent interfaces is generally well represented by atomistic models based on classical potentials. However, the atomistic approach to investigating semicoherent interfaces is not well suited to high-throughput studies. For example, given that it takes at best several hours to construct, relax, and analyze a single atomistic interface model, investigations of the full, five-parameter space of interface crystallographic character would take several decades. To make high-throughput investigations feasible, we have undertaken to develop a much faster model of semicoherent interface structure: one that does not track atomic positions, but rather only the dislocations that compose the interface. The goal of this model is to enable rapid scanning over the space of interface crystallographic characters while retaining a level of precision suitable to the application of interest.

Our model is based on the quantized Frank-Bilby equation (qFBE) and anisotropic linear elasticity theory [2]–[4]. The qFBE relates the crystallographic character of an interface to its Burgers vector content. For any interface, it provides a set of candidate dislocation network structures that are consistent with the prescribed crystallography. The linear elasticity component of our model computes the elastic strain energy of each of these solutions. We select the solution with lowest elastic strain energy as the structure most likely to be encountered in a full atomistic model of the interface of interest.

We have compared our predictions with atomistic simulations of fcc/bcc interfaces formed along the closest-packed planes of the neighboring crystals. We obtained excellent agreement in the interface structures found by these models [2]. More surprisingly, the elastic energies predicted by the dislocation-based model were often in quantitative agreement with the relative interface energies computed from the full atomistic models. Such agreement was not initially expected, as the dislocation-based model is a "minimal" description of the interface that ignores many important factors, such as dislocation core energies, dislocation network relaxations, and elastic nonlinearities. The success of this model gives hope that fast, semi-quantitative predictions of the structure, energy, and physical properties of general interfaces may be achieved without resorting to full atomistic models.

REFERENCES

[1] I.J. Beyerlein, M.J. Demkowicz, A. Misra, B.P. Uberuaga, *Defect-interface interactions*, Prog. Mater. Sci. **74** (2015), 125–210.
[2] A.J. Vattré, N. Abdolrahim, K. Kolluri, M.J. Demkowicz, *Computational design of patterned interfaces using reduced order models*, Scientific Reports **4** (2014), 6231.
[3] A.J. Vattré, M.J. Demkowicz, *Determining the Burgers vectors and elastic strain energies of interface dislocation arrays using anisotropic elasticity theory*, Acta Mater. **61** (2013), 5172–5187.
[4] N. Abdolrahim, M.J. Demkowicz, *Determining coherent reference states of general semicoherent interfaces*, Computational Materials Science, (2016), in print.

Topology and hysteretic domain-wall transitions in ferromagnets

Lukas Döring
(joint work with Radu Ignat, Felix Otto)

Let $x = (x_1, x_3) \in \Omega := \mathbb{R} \times (-1, 1)$ and consider $m \in \dot{H}^1(\Omega, \mathbb{S}^2)$ such that for $m' = (m_1, m_3)$, we have

$$\nabla \cdot m' = \partial_1 m_1 + \partial_3 m_3 = 0 \quad \text{in } \Omega, \quad m_3 = 0 \quad \text{on } \partial\Omega.$$

Moreover, for $m_\theta^\pm := (\cos\theta, \pm\sin\theta, 0)$, $\theta \in [0, \frac{\pi}{2}]$, we introduce the notation

$$m(\pm\infty, \cdot) = m_\theta^\pm \quad \overset{\text{Def.}}{\Longleftrightarrow} \quad \int_{\{x_1 > 0\}} |m - m_\theta^+|^2 dx + \int_{\{x_1 < 0\}} |m + m_\theta^-|^2 dx < \infty$$

and let

$$M_\theta := \left\{ m \in \dot{H}^1(\Omega; \mathbb{S}^2) \ \middle| \ \nabla \cdot m' = 0 \text{ in } \Omega, \ m_3 = 0 \text{ on } \partial\Omega, \ m(\pm\infty, \cdot) = m_\theta^\pm \right\}.$$

To any $m \in M_\theta$, we can associate both a "degree"

$$D(m) := \tfrac{1}{2\pi} \int_\Omega m \cdot \partial_1 m \times \partial_3 m \, dx \in \mathbb{Z}$$

and a "winding number"

$$W(m) := \tfrac{1}{\pi} \int_\Omega \nabla m_1 \times \nabla m_2 \, dx \in \mathbb{Z}.$$

We may now ask the following question (see also [1, 2]) that will be addressed in a forthcoming paper:

Question: Is

$$\inf \left\{ \int_\Omega |\nabla m|^2 dx \ \middle| \ m \in M_\theta, \ Q(m) = q \right\}$$

attained for all $\theta \in (0, \frac{\pi}{2}]$ and $q \in \{-1, 0, 1\}$, where Q denotes either the degree D or the winding number W? What about a general $q \in \mathbb{Z}$?

The above problem arises in the analysis of the internal structure of domain walls in soft ferromagnetic films. Domain walls are transition layers that separate regions ("domains") of constant magnetization directions $m_\theta^\pm$. By Ω, we denote the cross-section in the $x_1 x_3$-plane of a ferromagnetic film that is infinitely extended in the $x_1 x_2$-plane.

A version of the aforementioned minimization problem without topological constraint appears in [1] as the Γ-limit of the micromagnetic energy functional

$$E_\eta(m) := \int_\Omega |\nabla m|^2 + \lambda \ln(\tfrac{1}{\eta}) \int_{\mathbb{R}^2} |h|^2 dx + \eta \int_\Omega (m_1 - H)^2 + m_3^2 \, dx,$$

for $\eta \downarrow 0$. Here, the stray field $h = -\nabla u \colon \mathbb{R}^2 \to \mathbb{R}^2$ solves Maxwell's equation

$$\nabla \cdot (h + m' \mathbf{1}_\Omega) = 0 \quad \text{in } \mathcal{D}'(\mathbb{R}^2).$$

Up to a logarithm, the parameter $\eta \ll 1$ denotes the quality factor of the anisotropy of the material, while $\lambda > 0$ may be interpreted as (non-dimensionalized) film

thickness. Finally, $H \in [0, 1]$ is the reduced strength of an external magnetic field along the x_1 direction.

In particular (see [1, Corollary 1]), we have for $H = \cos \alpha$, $\alpha \in (0, \frac{\pi}{2}]$, that

$$\min \left\{ E_\eta(m) \mid m \colon \Omega \to \mathbb{S}^2, \ m(\pm\infty, \cdot) = m_\alpha^\pm \right\}$$
$$\overset{\eta \downarrow 0}{\to} \min_{\theta \in [0, \frac{\pi}{2}]} \left(\min_{m \in M_\theta} \int_\Omega |\nabla m|^2 dx + 2\pi \lambda \left(\cos \theta - H \right)^2 \right).$$

On the level of the wall energy and in a certain regime of film thicknesses, the result confirms the prediction [4] that the favored domain walls are an optimal combination of a stray-field free wall core (corresponding to the first term of the limit energy) and logarithmic wall tails (corresponding to the second term of the limit energy).

Numerically, one can identify two critical points of the "exchange energy integral" $\int_\Omega |\nabla m|^2 dx$ in M_θ that correspond to transition layers that are called asymmetric Néel and asymmetric Bloch wall, respectively. Both are known in physics since the late 1960s. [3, 4]

Since these numerical solutions clearly have different degrees and winding numbers, it is natural to ask whether both wall types are local minimizers in their respective topological classes.

A related question concerns the stability of those wall types: In numerical simulations [5] and experiments [6], hysteretic transitions between asymmetric Néel and Bloch walls are observed under a varying external field H. From a theoretical point of view, this hysteresis has not yet been explained. In particular, the transition fields H_{BN} and H_{NB} that mark the transition from Bloch to Néel wall and vice versa, are not known.

If both asymmetric wall types are global minimizers of the exchange energy in their topological class, i.e., local minimizers of the exchange energy in M_θ without topological constraint, one cannot expect a continuous transition between these wall types in the leading-order Γ-limit of the Landau-Lifshitz energy E_η. Hence, either a higher-order expansion that allows for non-zero normal component m_3 on $\partial\Omega$ or some other mechanism of instability has to be considered.

References

[1] L. Döring, R. Ignat, F. Otto, *A reduced model for domain walls in soft ferromagnetic films at the cross-over from symmetric to asymmetric wall types*, J. Eur. Math. Soc. **16** (2014), 1377–1422.

[2] L. Döring, R. Ignat, *Asymmetric domain walls of small angle in soft ferromagnetic films*, Arch. Rat. Mech. Anal. **220** (2016), 889–936.

[3] A. E. LaBonte, *Two-dimensional Bloch-type domain walls in ferromagnetic films*, J. Appl. Phys. **40** (1969), 2450–2458.

[4] A. Hubert, *Stray-field-free magnetization configurations*, phys. stat. sol. **32** (1969), 519–534.

[5] S. W. Yuan, H. N. Bertram, *Domain-wall dynamic transitions in thin films*, Phys. Rev. B **44** (1991), 12395–12405.

[6] L. Döring, C. Hengst, F. Otto, R. Schäfer, *Interacting tails of asymmetric domain walls: theory and experiments*, Phys. Rev. B **93** (2016), 024414.

A phase-field model of dislocations on several slip planes

Peter Gladbach

(joint work with Sergio Conti)

We extend the Peierls-Nabarro model of crystallographic slip developed in [1] to multiple parallel slip planes $\omega_{h^m} = \omega \times \{h^m\}$ in an elastic medium $\Omega = \omega \times \mathbb{R}$, where $\omega \subset \mathbb{R}^2$ and $M \in \mathbb{N}$, $h^1 < \ldots < h^M \in \mathbb{R}$. The normal to the slip planes in this case is e_3 but can be any unit vector by rotation. We allow crystallographic slips $b^m : \omega_{h^m} \to \mathbb{R}^2$ in tangential direction on each slip plane, where we penalize deviations from the Burgers lattice $\mathcal{B} \approx \mathbb{Z}^2 \subset \mathbb{R}^2$ with a Peierls potential

$$(1) \qquad E_\varepsilon^{\text{Peierls}}[b^1, \ldots, b^M] = \frac{1}{\varepsilon} \sum_{m=1}^{M} \int_{\omega_{h^m}} \text{dist}^2(b^m, \mathbb{Z}^2) \, d\mathcal{H}^2.$$

Additionally there is a nonlocal elastic interaction term due to nonconstant slip fields. More precisely, the boundaries between regions of different slips are dislocations, which induce long-range elastic stress in the bulk Ω. We characterize the interaction in terms of an optimal displacement field $u : \Omega \setminus \bigcup_{m=1}^{M} \omega_{h^m} \to \mathbb{R}^3$ as

$$(2) \quad E_{h^1, \ldots, h^M}^{\text{elastic}}[b^1, \ldots, b^m] = \inf \left\{ \int_{\Omega \setminus \bigcup_{m=1}^{M} \omega_{h^m}} \mathbb{C} Eu \cdot Eu \, dx \, : \, [u] = b^m \text{ on } \omega_{h^m} \right\},$$

where $[u] = T^+u - T^-u$ denotes the jump of u in the sense of the difference of its two traces. The total energy in terms of the slip vector field $\boldsymbol{b} = (b^1, \ldots, b^M) : \omega \to \mathbb{R}^{2M}$ is then $E_{\varepsilon, h^1, \ldots, h^M}[\boldsymbol{b}] = E_\varepsilon^{\text{Peierls}}[\boldsymbol{b}] + E_{h^1, \ldots, h^M}^{\text{elastic}}[\boldsymbol{b}]$. Note that this constitutes a 2-dimensional model, as $\sum_{m=1}^{M} \text{dist}^2(b^m, \mathbb{Z}^2) = \text{dist}^2(\boldsymbol{b}, \mathbb{Z}^{2M})$, and the elastic interaction can be written as

$$(3) \quad E_{h^1, \ldots, h^M}^{\text{elastic}}[\boldsymbol{b}] = \int_\omega \int_\omega (\boldsymbol{b}(x) - \boldsymbol{b}(y)) \mathbb{J}_{h^1, \ldots, h^M}(x - y)(\boldsymbol{b}(x) - \boldsymbol{b}(y)) \, d\mathcal{H}^2(x) \, d\mathcal{H}^2(y),$$

with $\mathbb{J}_{h^1, \ldots, h^M} : \mathbb{R}^2 \to \mathbb{R}^{nM \times nM}$.

We investigate the asymptotic behavior of $E_{\varepsilon, h^1, \ldots, h^M}[\boldsymbol{b}]/|\log \varepsilon|$ to develop a line-tension limit. The limit energy for a single plane, in the sense of Γ-convergence, was shown in [2] to be the functional defined on the space $BV(\omega, \mathbb{Z}^2)$ given by

$$(4) \qquad I_{LT}[b] = \int_{S_b} \varphi^{\text{rel}}([b], \nu) \, d\mathcal{H}^1,$$

where $S_b \subset \omega$ denotes the jump set of b, $[b] \in \mathbb{Z}^2$ the magnitude of its jump, and $\nu \in S^1$ its in-plane normal. The energy density $\varphi^{\text{rel}} : \mathbb{Z}^2 \times S^1 \to [0\infty)$ is the BV-elliptic envelope of the self-energy of a straight dislocation line $\varphi : \mathbb{Z}^2 \times S^1 \to [0, \infty)$. The relaxation operation accounts for dislocation microstructure. For multiple planes, the limit energy as $\varepsilon \to 0$ and $h^{m+1} - h^m \to 0$ varies with their scaling relation. For ease of notation we assume $h^m = mh$, where $h \to 0$ denotes the spacing between adjacent planes. We obtain the compactness result

Theorem 1 ([3]). *Assume $\varepsilon_k \downarrow 0$, $h_k \geq 0$. Assume that $\boldsymbol{b}_k$ is a sequence of slip vector fields with $\liminf_{k \to \infty} E_{\varepsilon_k, h_k, \ldots, Mh_k}[\boldsymbol{b}_k]/|\log \varepsilon| < \infty$. Then*

i) *If* $\liminf_{k\to\infty} \frac{\log h_k}{\log \varepsilon_k} < 1$, *there is a subsequence such that up to a constant* $\boldsymbol{b}_{k_j}$ *converges in* $L^1(\omega, \mathbb{R}^{2M})$ *to a slip vector field* $\boldsymbol{b} \in BV(\omega, \mathbb{Z}^{2M})$.

ii) *If* $\liminf_{k\to\infty} \frac{\log h_k}{\log \varepsilon_k} \geq 1$ *there is a subsequence such that up to a constant the sum of slips* $\sum_{m=1}^{M} b_{k_j}^m$ *converges in* $L^1(\omega, \mathbb{R}^2)$ *to some* $b \in BV(\omega, \mathbb{Z}^2)$.

Here the first case corresponds to a well-separatedness between the planes, e.g. $h \approx \varepsilon^\beta$ for some $\beta < 1$. In the second case, corresponding roughly to $h = O(\varepsilon)$, we can only recover the sum of all slips. The limit energy features interactions between jumps of different slip fields as long as they are very close, with the strength of the interaction varying with $\beta = \lim_{k\to\infty} \frac{\log h_k}{\log \varepsilon_k}$:

Theorem 2 ([3]). *Assume* $\varepsilon_k \downarrow 0$, $h \geq 0$, $\beta \in [-\infty, \infty]$ *exists. Then* $E_{\varepsilon_k, h_k, \ldots, Mh_k} / |\log \varepsilon_k|$ Γ-*converges to a line-tension functional defined on the space* $BV(\omega, \mathbb{Z}^{2M})$ *given by*

$$(5) \qquad I_{LT}[\boldsymbol{b}] = \int_{S_{\boldsymbol{b}}} \varphi_\beta^{\mathrm{rel}}([\boldsymbol{b}], \nu) \, d\mathcal{H}^1,$$

where

i) *For* $\beta \leq 0$, $\varphi_\beta^{\mathrm{rel}}$ *is the* BV-*elliptic envelope* $\varphi_{\mathrm{short}}^{\mathrm{rel}}$, *where* $\varphi_{\mathrm{short}} : \mathbb{Z}^{2M} \times S^1 \to [0, \infty)$ *is the short-range self-energy*

$$(6) \qquad \varphi_{\mathrm{short}}(\boldsymbol{B}, \nu) = \sum_{m=1}^{M} \varphi(B^m, \nu),$$

$$(7) \qquad \varphi_{\mathrm{short}}^{\mathrm{rel}}(\boldsymbol{B}, \nu) = \sum_{m=1}^{M} \varphi^{\mathrm{rel}}(B^m, \nu).$$

ii) *For* $\beta \geq 1$, $\varphi_\beta^{\mathrm{rel}}$ *is the* BV-*elliptic envelope* $\varphi_{\mathrm{long}}^{\mathrm{rel}}$, *where* $\varphi_{\mathrm{long}} : \mathbb{Z}^{2M} \times S^1 \to [0, \infty)$ *is the long-range self-energy*

$$(8) \qquad \varphi_{\mathrm{long}}(\boldsymbol{B}, \nu) = \varphi\left(\sum_{m=1}^{M} B^m, \nu\right),$$

$$(9) \qquad \varphi_{\mathrm{long}}^{\mathrm{rel}}(\boldsymbol{B}, \nu) = \varphi^{\mathrm{rel}}\left(\sum_{m=1}^{M} B^m, \nu\right).$$

iii) *For* $\beta \in (0, 1)$, $\varphi_\beta^{\mathrm{rel}}$ *is the double relaxation*

$$(10) \qquad \varphi_\beta^{\mathrm{rel}} = \left[(1 - \beta)\varphi_{\mathrm{short}}^{\mathrm{rel}} + \beta\varphi_{\mathrm{long}}\right]^{\mathrm{rel}}.$$

The double relaxation for the intermediate scalings $\beta \in (0, 1)$ is realized by a two-scale microstructure. For examples where complex microstructures arise, see [4].
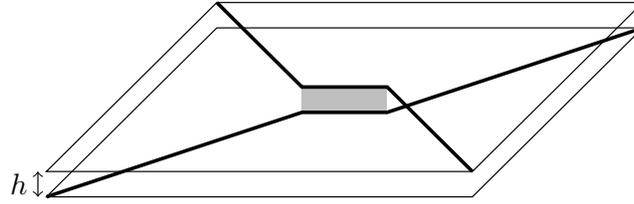
FIGURE 1. The limit energy is concentrated on the dislocation lines. Dislocations in different planes will interact whenever they run in parallel.

REFERENCES

[1] M. Koslowski, A. M. Cuitiño, M. Ortiz, *A phase-field theory of dislocation dynamics, strain hardening and hysteresis in ductile single crystal*, J. Mech. Phys. Solids **50** (2002), 2597–2635.
[2] S. Conti, A. Garroni, S. Müller, *Singular kernels, multiscale decomposition of microstructure, and dislocation models*, Arch. Ration. Mech. Anal. **199** (2011), 779–819.
[3] P. Gladbach, *Line-tension models for dislocations in crystals*, Ph.D. thesis, Universität Bonn (in preparation).
[4] S. Conti and P. Gladbach, *A line-tension model of dislocation networks on several slip planes*, Mechanics of Materials **90** (2015), 140–147.

The spectral decomposition of the stiffness hexadic in gradient elasticity

RAINER GLÜGE

(joint work with Jan Kalisch, Albrecht Bertram)

1. INTRODUCTION

It is well known that classical elasticity cannot account for size effects that are observed in very small structures [1, 2]. Mostly, the specific stiffness of fine structures is increased. It is also well known that one can overcome this shortcoming by including a strain gradient dependence in the elastic energy. The isotropic extension of linear elasticity has been given by [3]. It involves a sixth-order stiffness tensor with five independent parameters,

$$
\begin{aligned}
\overset{\langle 6 \rangle}{\mathbb{C}} = \big[& c_1(\delta_{jk}\delta_{im}\delta_{nl} + \delta_{jk}\delta_{in}\delta_{ml} + \delta_{ji}\delta_{kl}\delta_{mn} + \delta_{jl}\delta_{ik}\delta_{mn}) + \\
& c_2(\delta_{ji}\delta_{km}\delta_{nl} + \delta_{jm}\delta_{ki}\delta_{nl} + \delta_{ji}\delta_{kn}\delta_{ml} + \delta_{jn}\delta_{ik}\delta_{ml}) + \\
& c_3(\delta_{jm}\delta_{kl}\delta_{in} + \delta_{jl}\delta_{in}\delta_{km} + \delta_{jn}\delta_{im}\delta_{kl} + \delta_{jl}\delta_{im}\delta_{nk}) + \\
& c_4(\delta_{jn}\delta_{il}\delta_{km} + \delta_{jm}\delta_{kn}\delta_{il}) + \\
& c_5\delta_{jk}\delta_{il}\delta_{mn} \big] \mathbf{e}_i \otimes \mathbf{e}_j \otimes \mathbf{e}_k \otimes \mathbf{e}_l \otimes \mathbf{e}_m \otimes \mathbf{e}_n
\end{aligned}
$$

which relates the second displacement gradient $\mathbf{u} \otimes \nabla \otimes \nabla$ to the corresponding hyperstress tensor. It has the index symmetries $C_{ijklmn} = C_{lmnijk} = C_{ijklnm} = C_{ikjlmn}$ w.r.t. an orthonormal basis. The aim of the present work is to give the spectral decomposition of this hexadic. Often, the strain gradient $\mathrm{sym}(\mathbf{u} \otimes \nabla) \otimes \nabla$ is used in place of the second displacement gradient. Both forms can be translated into each other [3].

2. Spectral decomposition of $\mathbb{C}$

We summarize the different combinations of Kronecker symbols that belong to each parameter c_i above with the basis $\{\mathbf{e}_i \otimes \mathbf{e}_j \otimes \mathbf{e}_k \otimes \mathbf{e}_l \otimes \mathbf{e}_m \otimes \mathbf{e}_n\}$ to five base hexadics $\{\mathbb{B}_i\}$, such that

$$\overset{\langle 6 \rangle}{\mathbb{C}} = \sum_{i=1}^{5} c_i \mathbb{B}_i.$$

The metric of the basis $\{\mathbb{B}_i\}$ is

$$\mathbb{B}_i \cdots\cdots \mathbb{B}_j = \begin{bmatrix} 168 & 96 & 96 & 24 & 36 \\ 96 & 192 & 72 & 48 & 12 \\ 96 & 72 & 192 & 48 & 12 \\ 24 & 48 & 48 & 72 & 18 \\ 36 & 12 & 12 & 18 & 27 \end{bmatrix}.$$

For the spectral decomposition, a mote suitable basis is introduced,

$$\tilde{\mathbb{B}}_1 := -\frac{1}{15}\left(\mathbb{B}_1 + \mathbb{B}_2 + \mathbb{B}_5\right) + \frac{1}{6}\left(\mathbb{B}_3 + \mathbb{B}_4\right)$$

$$\tilde{\mathbb{B}}_2 := \frac{1}{12}\left(2\,\mathbb{B}_1 - \mathbb{B}_2 - 2\,\mathbb{B}_3 + 4\,\mathbb{B}_4 - 4\,\mathbb{B}_5\right)$$

$$\tilde{\mathbb{B}}_3 := \frac{1}{60}(6\,\mathbb{B}_1 - 9\,\mathbb{B}_2 + 16\,\mathbb{B}_5)$$

$$\tilde{\mathbb{B}}_4 := \frac{1}{6\sqrt{5}}\left(3\,\mathbb{B}_1 - 4\,\mathbb{B}_5\right)$$

$$\tilde{\mathbb{B}}_5 := \frac{1}{20}(-2\,\mathbb{B}_1 + 3\,\mathbb{B}_2 + 8\,\mathbb{B}_5).$$

The metric of this basis is diagonal with $\tilde{\mathbb{B}}_i \cdots\cdots \tilde{\mathbb{B}}_i = (7, 5, 6, 6, 6)$. The components of $\overset{\langle 6 \rangle}{\mathbb{C}}$ with respect to this basis are

$$\tilde{c}_1 := 2\left(c_4 - c_3\right) \qquad\qquad\qquad \tilde{c}_2 := 4\,c_3 + 2\,c_4$$

$$\tilde{c}_3 := \frac{1}{6}\left(12\,c_1 - 16\,c_2 + 2\,c_3 + 9\,c_5\right)$$

$$\tilde{c}_4 := \frac{2\sqrt{5}}{3}\left(3\,c_1 + 2\,c_2 + 2\,c_3\right)$$

$$\tilde{c}_5 := \frac{1}{2}(4\,c_1 + 8\,c_2 + 2\,c_3 + 4\,c_4 + 3\,c_5).$$

Eigenvalues and projectors: In terms of the latter basis $\{\tilde{\mathbb{B}}_i\}$ and components $\tilde{c}_i$, the spectral decomposition of $\overset{\langle 6 \rangle}{\mathbb{C}}$ is given by

$$\overset{\langle 6 \rangle}{\mathbb{C}} = \sum_{i=1}^{4} \lambda_i \mathbb{P}_i$$

with the eigenvalues

$$\lambda_1 = \tilde{c}_1 \qquad\qquad\qquad \lambda_2 = \tilde{c}_2$$
$$\lambda_3 = \tilde{c}_5 + c_r \qquad\qquad \lambda_4 = \tilde{c}_5 - c_r$$

with

$$c_r = \sqrt{\tilde{c}_3^2 + \tilde{c}_4^2}$$

and the eigenprojectors

$$\mathbb{P}_1 = \tilde{\mathbb{B}}_1$$
$$\mathbb{P}_2 = \tilde{\mathbb{B}}_2$$
$$\mathbb{P}_3(\kappa) = \frac{1}{2}(\tilde{\mathbb{B}}_5 + \frac{\tilde{c}_3}{c_r}\tilde{\mathbb{B}}_3 + \frac{\tilde{c}_4}{\tilde{c}_r}\tilde{\mathbb{B}}_4)$$
$$\mathbb{P}_4(\kappa) = \frac{1}{2}(\tilde{\mathbb{B}}_5 - \frac{\tilde{c}_3}{c_r}\tilde{\mathbb{B}}_3 - \frac{\tilde{c}_4}{\tilde{c}_r}\tilde{\mathbb{B}}_4)$$

with

$$\cos\kappa = \frac{\tilde{c}_3}{c_r} \qquad \Leftrightarrow \qquad \sin\kappa = \frac{\tilde{c}_4}{c_r}.$$

For the spectral decomposition, the representation of $\overset{\langle 6 \rangle}{\mathbb{C}}$ with the dimensionless parameter κ and the four eigenvalues is more convenient than with the parameters $\{c_1, c_2, c_3, c_4, c_5\}$ or $\{\tilde{c}_1, \tilde{c}_2, \tilde{c}_3, \tilde{c}_4, c_r\}$. One can check that

$$\mathbb{P}_3(\kappa) = \mathbb{P}_4(\kappa + \pi)$$
$$\lambda_3(\kappa) = \lambda_4(\kappa + \pi)$$

holds, i.e., it is reasonable to restrict κ to the interval $[0, \pi)$. The metric of the projectors is diagonal with $\mathbb{P}_i \cdots\cdots \mathbb{P}_i = (7, 5, 3, 3)$, thus the multiplicities of the eigenvalues are 7, 5, 3 and 3. Further, we have the projector properties

$$\mathbb{P}_i \cdots \mathbb{P}_j = \begin{cases} \mathbb{P}_i \text{ if } i = j \\ \mathbb{O} \text{ if } i \neq j \end{cases}$$

$$\sum_{i=1}^{4} \mathbb{P}_i = \mathbb{I},$$

where $\mathbb{I}$ is the sixth-order identity tensor on triads with the right subsymmetry. These equations resemble those of the spectral decomposition of a transversely isotropic stiffness tetradic (see Appendix A of [1]), which also has in general five independent components and four distinct eigenvalues.

The above formulae are convenient when one knows the parameters $c_{1,2,3,4,5}$, and seeks the eigenvalues and the third and fourth eigenprojector. The other way around, the coefficients $c_{1,2,3,4,5}$ are given by

$$c_1 = (10\lambda_1 - 4\lambda_2 - 3(\lambda_3 + \lambda_4) + 3(\lambda_3 - \lambda_4)(\cos(\kappa) + \sqrt{5}\sin(\kappa)))/60$$
$$c_2 = (-10\lambda_1 - 8\lambda_2 + 9(\lambda_3 + \lambda_4) + 9(-\lambda_3 + \lambda_4)\cos(\kappa))/120$$
$$c_3 = (-\lambda_1 + \lambda_2)/6$$
$$c_4 = (2\lambda_1 + \lambda_2)/6$$
$$c_5 = (-5\lambda_1 - \lambda_2 + 3(\lambda_3 + \lambda_4) + (\lambda_3 - \lambda_4)(2\cos(\kappa) - \sqrt{5}\sin(\kappa)))/15$$

in terms of $\{\lambda_{1,2,3,4}, \kappa\}$.

References

[1] J. Kalisch, R. Glüge, *Analytical homogenization of linear elasticity based on the interface orientation distribution – a complement to the self-consistent approach*, Composite Structures **126** (2015), 398–416.
[2] C. Liebhold, W. Müller, *Measuring Material Coefficients of Higher Gradient Elasticity by Using AFM Techniques and Raman-Spectroscopy*, Generalized Continua as Models for Materials **22** (2013), 255–271 Series: Advanced Structured Materials, Editors: H. Altenbach, S. Forest, A. Krivtsov.
[3] R.D. Mindlin, *Micro-structure in linear elasticity*, Archive for Rational Mechanics and Analysis **16** (1964), 51–78.

Continuum dislocation dynamics: current state and open topics

THOMAS HOCHRAINER

(joint work with Alireza Ebrahimi, Stefan Sandfeld, Michael Zaiser)

Crystal plasticity is mediated by the motion of line like crystal defects, the dislocations. Although the behavior of individual dislocations and dislocation interactions are reasonably well understood, no continuum plasticity has yet been established which results from a controlled averaging procedure for dislocations. Continuum dislocation dynamics (CDD) is a recently developed theory, which characterizes the dislocation state of a crystal by a hierarchy of dislocation density alignment tensors and curvature density tensors which evolve according to non-standard conservation laws [1].

In order to define from continuum dislocation dynamics a crystal plasticity materials law, constitutive equations for the average dislocation speed v are required. For straight parallel edge dislocations such a constitutive law could be derived from direct averaging of the dislocation dynamics [2] by closing a BBGKY hierarchy at low order. As a result, two mesoscopic shear stresses were found to determine the dislocation velocity besides the resolved shear stress τ: a Taylor type flow stress (friction stress) $\tau_{\mathrm{f}} = \alpha G b \sqrt{\rho}$ and a back stress $\tau_{\mathrm{b}} = DGb\partial_x^2\gamma/\rho$. Here, ρ denotes the total dislocation density, γ the accumulated plastic shear, α and D are dimensionless constants, G denotes the shear modulus, b is the modulus of the Burgers vector and the x-coordinate points in the direction of the Burgers vector. With

the net-shear stress defined as $\tau_{\text{net}} = \tau - \tau_{\text{b}}$ the average dislocation velocity is taken to be of the form $v = Mb \operatorname{sign}(\tau_{\text{net}}) \langle |\tau_{\text{net}}| - \tau_{\text{f}} \rangle$, where M is a dislocation mobility, sign returns the signature of its argument and $\langle \cdot \rangle$ denote the Macaulay brackets, which return their argument if its positive and zero else. The derivation of these terms was possible because the pair correlations of the quasi 2D dislocation positions, which were obtained from 2D discrete dislocation simulations, turned out to be short ranged. For curved dislocations it seems unpractical to obtain pair correlations because the amount of statistics which would be needed is hardly accessible from 3D discrete dislocation simulations. An alternative to averaging the dynamics is to obtain an energy density expression of a dislocation system in terms of the dislocation density variables, i.e. via a local density approximation, and to derive the constitutive law for the average dislocation velocity from the requirement of thermodynamic consistency combined with thermodynamic extremal principles.

Recently, Zaiser [3] presented a derivation of a local density approximation for general dislocation systems using the lowest order dislocation alignment tensors (up to order 2) as density variables. A crucial assumption in this derivation is that also the pair correlations in systems of curved dislocations are short ranged. Under this assumption the free energy density splits into an elastic and a defect related part. In terms of the total dislocation density ρ, the dislocation density vector $\boldsymbol{\rho} = \mathbf{n} \times \nabla\gamma$ ($\mathbf{n}$ denotes the slip plane normal), and the scalar curvature density q the energy density is of the form

$$
(1) \quad \Psi(\mathbf{x}) = \boldsymbol{\epsilon}^{\text{el}}(\mathbf{x}) : \mathbf{C} : \boldsymbol{\epsilon}^{\text{el}}(\mathbf{x})
$$
$$
+ \frac{Gb^2}{8\pi} \left[\frac{(2-\nu)}{(1-\nu)} \rho(\mathbf{x}) \ln\left(\frac{\rho(\mathbf{x})}{Aq(\mathbf{x})b} \right) + \frac{\boldsymbol{\rho}(\mathbf{x}) \cdot \mathbf{D} \cdot \boldsymbol{\rho}(\mathbf{x})}{\rho(\mathbf{x})} \right].
$$

Herein $\boldsymbol{\epsilon}^{\text{el}}$ denotes the elastic strain, $\mathbf{C}$ is the tensor of elastic moduli, ν is Poisson's ratio, A is a dimensionless constant, and $\mathbf{D}$ is a dimensionless tensor of second order. The dimensionless constants result from correlations in the system. The form of the energy in (1) is not unexpected and generalizes an expression suggested by Groma for straight parallel edge dislocations from scaling arguments. We note that the term containing the dislocation density vector strongly resembles energy expressions suggested in phenomenological strain gradient theories, since $\boldsymbol{\rho}$ is a first order strain gradient.

Though the energy (1) may not yet be the final word with regard to the dependence on q, it is instructive to use the conservation laws for the dislocation variables to obtain a thermodynamically consistent form of the dislocation velocity. This was done in [4], based on the evolution equations for the lowest order density variables (including plastic shear) on a single slip system

$$
\begin{aligned}
\dot{\gamma} &= \rho v b \\
\dot{\rho} &= \nabla \cdot (-v\mathbf{n} \times \boldsymbol{\rho}) + vq \\
\dot{\boldsymbol{\rho}} &= \nabla \times (v\rho\mathbf{n}) \\
\dot{q} &= \nabla \cdot \left(v\mathbf{q} - \boldsymbol{\rho}^{(2)} \cdot \nabla v \right).
\end{aligned}
$$

In the evolution equation for q appear the curvature vector $\mathbf{q}$ and the second order dislocation alignment tensor $\boldsymbol{\rho}^{(2)}$, which both have to be determined by closure assumptions from the other variables, compare [1, 5].

For an infinite body, partial integration yields the driving force for the dislocations expressed through mesoscopic shear stresses as [4]

$$(2) \quad \tau_{\text{net}} \quad = \quad \tau + \frac{1}{\rho b} \left\{ -\nabla \gamma \cdot \nabla \frac{\partial \Psi}{\partial \rho} - q \frac{\partial \Psi}{\partial \rho} - \rho \nabla \cdot \left(\mathbf{n} \times \frac{\partial \Psi}{\partial \boldsymbol{\rho}} \right) \right. $$
$$\left. + \mathbf{q} \cdot \frac{\partial \Psi}{\partial q} + \nabla \cdot \left(\boldsymbol{\rho}^{(2)} \cdot \nabla \frac{\partial \Psi}{\partial q} \right) \right\}. $$

The mesoscopic shear stresses in the curly braces partially show an expected form. The third term in the braces in (2) corresponds to the back stress in the theory of Groma and would be viewed as the divergence of a microstress in the parlance of phenomenological strain gradient theory. The second term may righteously be interpreted as a line tension term yielding a tendency to reduce the curvature of the dislocations. The first term is remarkable because this also appears in the theory of straight dislocations, where it was not derived from averaging the forces. The last two terms are related to the curvature density-dependence of the free energy and are as of yet not well understood.

Through the provision of a local density approximation for continuum dislocation dynamics, the above sketched theory provides the first statistical continuum theory of curved dislocations. The theory has been implemented as a crystal plasticity subroutine (UMAT) for Abaqus in conjunction with the crystal plasticity framework DAMASK [6]. First results of micro-bending simulations have been presented in [7]. These results show unique features of the CDD theory, most notably in that the consideration of dislocation fluxes leads to effects which seem unexpected when viewed from more traditional continuum plasticity. For example, the dislocation density is usually found to be low where plastic slip is high – which is consistent with discrete dislocation dynamics simulations but is opposed to the usual assumption that plastic slip increases the dislocation density.

As already noted, continuum dislocation dynamics has become a statistical continuum theory for curved dislocations – at least for single slip situations on small scales and for relative small deformations. However, CDD is not yet a general theory of single crystal plasticity. A crucial point missing in the energetic approach is a derivation of the flow stress τ_{f}. Our current interpretation of this friction-type stress is that it accounts for a microscopic roughness of the energy landscape, which is lost in the local density approximation. Besides the 'hight' of the roughness which determines the flow stress, a rugged energy landscape may also show anisotropies which might lead to deviations from the thermodynamic extremal principle which is used to determine the 'flux direction' in the space of internal variables. With regard to the most prominent problem in plasticity, i.e. work hardening, the essential feature missing in CDD is a convincing concept for the evolution and activation of dislocation sources; be it through cross-slip,

dislocation reactions or jogs from dislocation cutting through each other. Moreover, the physics of dislocations interacting with surfaces and interfaces is as yet incompletely understood even on the microscopic level.

References

[1] T. Hochrainer, *Multipole expansion of continuum dislocations dynamics in terms of alignment tensors*, Philos. Mag. **95**(12) (2015), 1321–1367.

[2] I. Groma, F. F. Csikor, M. Zaiser, *Spatial correlations and higher-order gradient terms in a continuum description of dislocation dynamics*, Acta Mater. **51** (2003), 1271–1281.

[3] M. Zaiser, *Local density approximation for the energy functional of three-dimensional dislocation systems*, Phys. Rev. B **92** (2015), 174120.

[4] T. Hochrainer, *Thermodynamically consistent continuum dislocation dynamics*, J. Mech. Phys. Solids **88** (2016), 12–22.

[5] M. Monavari, S. Sandfeld, M. Zaiser, *Continuum Representation of Systems of Dislocation Lines: A General Method for Deriving Closed-Form Evolution Equations*, ArXiv e-prints, September 2015.

[6] F. Roters, P. Eisenlohr, C. Kords, D.D. Tjahjanto, M. Diehl, D. Raabe, *DAMASK: the Düsseldorf Advanced MAterial Simulation Kit for studying crystal plasticity using an FE based or a spectral numerical solver*, Symposium on Linking Scales in Computations: From Microstructure to Macro-scale Properties, Procedia IUTAM **3** (2012), 3–10.

[7] Alireza Ebrahimi and Thomas Hochrainer. *Three-dimensional continuum dislocation dynamics simulations of dislocation structure evolution in bending of a micro-beam*, MRS Advances, FirstView **2** (2016), 1–6.

Self-organizing processes in rubbers microstructure

Jörn Ihlemann

(joint work with Hans Wulf)

In some cases of evolving microstructures of materials self-organization processes play an important role. Sometimes this is more or less obvious like in the case of semi-crystalline plastics. In other cases like rubber materials the self-organization processes are only recognizable considering the macroscopic material behavior.

This works focusses on the self-organizing linkage patterns within rubber materials [1], which causes important macroscopic material characteristics. However, there are also some first results to predict grain refinement processes within the polycrystalline microstructure of metals. This is done with the help of the Continuum Dislocation Theory [2].

In the case of typical rubber materials the microstructure seems to evolve with every change in the loading but also during relaxation and creep phases. Industrially used filled rubber materials show large deformation capability, highly nonlinear material behavior as well as complicated inelastic effects, namely hysteresis even in stationary cycles, and a distinct softening induced by the loading-history, which is called Mullins effect. The induced softening is related to the direction of the prestrain and therefore Mullins effect results in a strain induced material anisotropy. Moreover, filled rubber exhibits viscous properties like relaxation and creeping with characteristic scaling effects. However, none of the molecular scale

components directly reproduces the macroscopic material behavior. Apparently, the typical rubber behavior emerges from the complex interaction of a large number of the basic components and their interactions.

In this work, rubber material behavior is explained by the theory of Self-Organizing Linkage Patterns (SOLP). It attributes the rubber behavior to the emergence of a pattern based on the weak physical interactions. The theory implies that, during an external deformation, a self-organization process of physical linkages starts on the molecular level. This leads to a separation of comparatively spacious, stiffened areas with to a great extend softened layers in between. Such a distribution of physical linkages is called linkage pattern and is interpreted as the origin of the influence of the loading history to the momentary material behavior. Mullins effect is attributed to an adaption of the pattern to previous deformation states. Relaxation is explained by a thermal decay of the pattern.

A very abstract model of rubbers microstructure has been coded (the so called Trial Program) and is employed to validate the SOLP-theory. Therein, the model elements represent abstract properties of the material components instead of single molecular entities. The program is capable of tracking the selforganized emergence of spatial structures which lead to anisotropic behavior. Moreover, the model is extended to incorporate the evolution of structures over time.

The model is evaluated by comparing simulated stress-strain curves to corresponding experimental results. Two-sided shear loading and multilevel relaxation loading can be simulated. The comparison with experimental data reveals a good qualitative reproduction of several typical filled rubber characteristics as nonlinearity, hysteresis and permanent set. Also Mullins effect with the induced anisotropy is successfully reproduced. In addition, the model exhibits the characteristic viscous properties of rubber like a weak velocity denpendency within cyclic processes, rounded cycles due to sinusoidal loadings and the typical scaling behavior within relaxation phases after cyclic loading. Moreover, the emergence and relevance of self-organized linkage patterns in the model can be clearly observed. These results give strong evidence, that self-organization is essential for rubber behavior and is a powerful approach for explaining how material properties emerge from molecular component properties.

References

[1] H. Wulf, J. Ihlemann, *Simulation of Mullins effect and relaxation due to self-organization processes in filled rubber*, in B. Marvalova, I. Petrikova (eds.), Constitutive models for rubber IX, CRC Press (2015), 305–310.

[2] C. B. Silbermann, J. Ihlemann, *Predicition of Self-organized dislocation patterns with continuum dislocation theory*, in A. Khan (ed.), Plastic Behavior of Conventional and Advanced Materials: Theory, Experiment, and Modeling, NEAT Press (2016), 49–51.

From atomistics to the continuum: bridging across scales and the quasicontinuum method

Dennis M. Kochmann

(joint work with Jeff Amelang, Gabriela Venturini, Ishan Tembhekar)

The limitations of available computational resources prevent the use of atomistic methods at technologically relevant length and time scales. At the same time, the continuum hypothesis, underlying all efficient continuum material models and kinematic descriptions, breaks down when characteristic problem sizes approach the nanoscale, such as in, e.g., nanocrystalline and nanoporous metals, nano-sized truss networks, or micro-/nano-electromechanical systems (MEMS/NEMS, respectively). Concurrent scale-bridging techniques are powerful tools to overcome those limitations by exporting atomistic accuracy to significantly larger length and time scales in an efficient manner and without assuming a separation of scales as in hierarchical methods. Coarse-graining techniques form a special class, in which the entire constitutive description (both in the discrete and the approximate continuum regions) is based on the lower-scale material model only (e.g., solely based on interatomic potentials without the need for empirical constitutive relations at the continuum scale).

One such technique, the *quasicontinuum* (QC) method [1] was introduced to coarse-grain crystalline atomistic ensembles in order to bridge across scales from individual atoms to the micro- and mesoscales. Various flavors of the QC method have been reported which differ by their local vs. nonlocal thermodynamic formulation, their approximation of the total Hamiltonian or of the interatomic forces, their interpolation schemes, and their model adaptation techniques, to name but a few. We recently introduced a new *fully-nonlocal QC method* [2, 3] which does not conceptually differentiate between atomistic and coarse-grained domains so as to enable a truly seamless scale-bridging from atomistics to the continuum. To this end, we introduce new, optimal energy-based summation rules that are based on a set of sampling atoms (different from the representative atoms) to approximate the total Hamiltonian. The resulting new QC approximation results in minimal approximation errors and thus in marginal residual and spurious force artifacts, as confirmed by benchmark examples in two and three dimensions. The new summation rule, similar in spirit to quadrature rules, allows for automatic model adaption and guarantees no force artifacts in the limits of full atomistic resolution as well as in large elements, and no residual forces in any affinely-strained ground state. Force artifacts only occur in the intermediate regime right above full atomistic resolution but are small compared to all previous schemes of comparable efficiency and bounded. Furthermore, we use a new model adaptation scheme which locally re-maps atomic neighborhoods so that the QC model can accurately represent large atomistic motion [4]. Automatic model refinement (based on an element-wise remeshing criterion) allows us to start with a considerably coarsened representation with the simulation code subsequently applying model adaptation wherever it is required (e.g., in the vicinity of defects). Thus, atomistic resolution

is tied to evolving regions of interest, e.g., around moving dislocations, propagating cracks, or expanding voids. The accuracy of the nonlocal QC method is confirmed in direct comparison with MD simulation results, as well as by proving the Γ-convergence of the energy-based QC formulation towards the same continuum limit as the exact atomistic model under quasistatic conditions [5].

We present selected examples of small-scale plasticity investigated by the new QC formulation. These include indentation tests as well as simulations of void growth and coalescence. Extensions to finite temperature introduce a separation of thermal fluctuations from the mean motions of repatoms, to be treated, e.g., by methods of statistical mechanics to interpret thermal oscillations as heat [6].

REFERENCES

[1] E. Tadmor, M. Ortiz, R. Philipps, *Quasicontinuum analysis of defects in solids*, Philos. Mag. A **73** (1996), 1529–1563.
[2] J. S. Amelang, G. N. Venturini, D. M. Kochmann, *Summation rules for a fully-nonlocal energy-based quasicontinuum method*, J. Mech. Phys. Solids **82** (2015), 378–413.
[3] J. S. Amelang, D. M. Kochmann, *Surface effects in nanoscale structures investigated by a fully-nonlocal energy-based quasicontinuum method*, Mech. Mater. **90** (2015), 166–184.
[4] I. Tembhekar, J. S. Amelang, D. M. Kochmann, *Automatic adaptivity in the fully-nonlocal quasicontinuum method for coarse-grained atomistic simulations*, Int. J. Num. Meth. Eng., submitted for publication (2016).
[5] M. Espanol, D. M. Kochmann, S. Conti, M. Ortiz. *A Γ-convergence analysis of the quasicontinumm method*, Multiscale Model. Simul. **11** (2013), 766–794.
[6] G. Venturini, K. Wang, I. Romero, M. P. Ariza, M. Ortiz, *Atomistic long-term simulation of heat and mass transport*, J. Mech. Phys. Solids **73** (2014), 242–268.

On the effective material response of bilayered composites in finite crystal plasticity

CAROLIN KREISBECK

(joint work with Fabian Christowiak)

Most elasto-plastic solids, such as metals, are polycrystalline, and therefore, on a mesoscopic level, assemblies of grains of differently oriented single crystals. Inside the grains, plastic deformation occurs by glide along selected slip systems, which are distinct directions of the crystal lattice. It has been observed in experiments that grain boundaries impose restrictions on still finer substructures, and highly influence the macroscopic material response. These effects have also been simulated and investigated in the literature, see e.g. [7, 6] and the references therein for an overview.

In this project, we intend to develop analytical tools that help characterize the effective material behavior of polycrystals in the context of finite-deformation plasticity. Our particular focus lies on the question of how the arrangement and geometry of the grains interact with the orientation of the active slip systems.

As a first step towards this complex problem, we make simplifying assumptions and study a variational model in two dimensions for composites made of fine parallel layers of two types. While one component is assumed to be completely
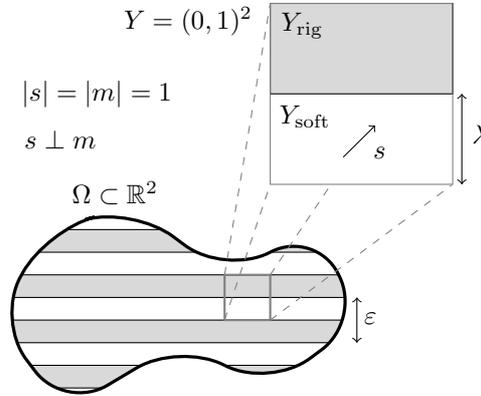
FIGURE 1. Bilayered composite material with stiff components.

rigid in the sense that it admits local rotations only, the other one is softer featuring a single active slip system (s, m) with linear self-hardening, see Figure 1. Here, $s \in \mathbb{R}^2$ with $|s| = 1$ stands for the slip direction, $m = s^\perp$ is the slip-plane normal, and the small parameter $\varepsilon > 0$ describes the length scale of the oscillations between the layers. For each ε, we consider the energy functional E_ε defined on deformations $u \in W^{1,2}(\Omega; \mathbb{R}^2)$ of the reference configuration $\Omega \subset \mathbb{R}^2$ by

$$E_\varepsilon(u) = \int_\Omega W\left(\frac{x}{\varepsilon}, \nabla u\right) \mathrm{d}x.$$

The density $W : \mathbb{R}^2 \times \mathbb{R}^{2 \times 2} \to [0, \infty]$ is given via periodic extension by

$$W(y, F) = W_{\mathrm{rig}}(F)\chi_{Y_{\mathrm{rig}}}(y) + W_{\mathrm{soft}}(F)\chi_{Y_{\mathrm{soft}}}(y), \qquad y \in Y, \ F \in \mathbb{R}^{2 \times 2},$$

where W_{rig} and W_{soft} are the condensed energy densities modeling the rigid and softer material components, respectively. For $U \subset \mathbb{R}^2$ the characteristic function χ_U takes the values 0 and ∞ in and outside of U. Inspired by the model for homogeneous single-slip materials without elasticity in [3, 2], one obtains

$$E_\varepsilon(u) = \int_\Omega |\nabla u m|^2 - 1 \ \mathrm{d}x \qquad \text{if } u \in W^{1,2}(\Omega; \mathbb{R}^2), \nabla u \in \mathcal{M}_s \text{ a.e. in } \Omega \text{ and}$$
$$\nabla u \in SO(2) \text{ a.e. in } \varepsilon Y_{\mathrm{rig}} \cap \Omega,$$

and we set $E_\varepsilon = \infty$ otherwise in $L_0^2(\Omega; \mathbb{R}^2)$, the space of $L^2(\Omega; \mathbb{R}^2)$-functions with zero mean value. Note that the set

$$\mathcal{M}_s := \{F \in \mathbb{R}^{2 \times 2} : F = R(\mathbb{I} + \gamma s \otimes m), R \in SO(2), \gamma \in \mathbb{R}\}$$

reflects the multiplicative decomposition of the deformation gradient in finite plasticity, with the rotations corresponding to the elastic part. In the plastic part $\mathbb{I} + \gamma s \otimes m$, the quantity $\gamma \in \mathbb{R}$ represents the amount of slip along (s, m).

Our main result provides a characterization of the effective limit model as $\varepsilon \to 0$, i.e., when the layers become finer and finer. Precisely, we derive an explicit homogenization formula by means of Γ-convergence, see e.g. [4] for a general introduction.

Owing to the anisotropic character of the problem, the findings depend decisively on how the slip direction is oriented with respect to the layers. In fact, our asymptotic analysis reveals three qualitatively different regimes, showing macroscopic shearing as well as blocking effects. For a detailed proof of the following theorem we refer to [1].

Theorem. *Let $\Omega \subset \mathbb{R}^2$ be a bounded Lipschitz domain. The Γ-limit of the family of functionals $(E_\varepsilon)_\varepsilon$ as $\varepsilon \to 0$ regarding the strong $L^2(\Omega; \mathbb{R}^2)$-topology is given by*

$$E(u) = \begin{cases} \dfrac{s_1^2}{\lambda} \displaystyle\int_\Omega \gamma^2 \, \mathrm{d}x - 2s_1 s_2 \int_\Omega \gamma \, \mathrm{d}x & \text{if } u \in W^{1,2}(\Omega; \mathbb{R}^2) \text{ such that} \\ & \quad \nabla u = R(\mathbb{I} + \gamma e_1 \otimes e_2) \text{ with } R \in SO(2), \\ & \quad \gamma \in L^2(\Omega), \ \gamma \in K_{s,\lambda} \text{ a.e. in } \Omega, \\ \infty & \text{otherwise}, \end{cases}$$

for $u \in L_0^2(\Omega; \mathbb{R}^2)$, where $K_{e_2,\lambda} = \{0\}$, $K_{e_1,\lambda} = \mathbb{R}$, and

$$K_{s,\lambda} = \begin{cases} [-2\frac{s_1}{s_2}\lambda, 0] & \text{if } s_1 s_2 > 0, \\ [0, -2\frac{s_1}{s_2}\lambda] & \text{if } s_1 s_2 < 0. \end{cases}$$

Also, sequences of bounded energy for $(E_\varepsilon)_\varepsilon$ are relatively compact in $L^2(\Omega; \mathbb{R}^2)$.

The factor $\frac{s_1^2}{\lambda}$, with $\lambda \in (0,1)$ denoting the relative thickness of the softer layers, constitutes an effective hardening modulus. Besides, it is interesting to observe that in the case of an inclined slip system, i.e. $s \notin \{e_1, e_2\}$, the limit functional E features a linear term in γ, which can be interpreted as a dissipative contribution.

When proving the Γ-convergence of $(E_\varepsilon)_\varepsilon$, technical difficulties arise from the differential inclusions that impose constraints on the energy functionals E_ε. This requires a careful analysis of the admissible microstructures, which entail a rather restricted class of possible macroscopic deformations. One of the key ingredients is an asymptotic rigidity result for deformations with gradients in $\mathcal{M}_s$ and $SO(2)$ on alternating strips, see [1] and below. It shows that, up to global rotation, the body is forced by the stiff layers into horizontal shearing.

Lemma. *If $(u_\varepsilon)_\varepsilon$ with $E_\varepsilon(u_\varepsilon) < C$ for all $\varepsilon > 0$ such that $u_\varepsilon \rightharpoonup u$ in $W^{1,2}(\Omega; \mathbb{R}^2)$, then*

$$\nabla u = R(\mathbb{I} + \gamma e_1 \otimes e_2)$$

where $R \in SO(2)$ and $\gamma \in L^2(\Omega)$ with $\partial_1 \gamma = 0$.

Finding optimal approximating deformations, or in other words recovery sequences, relies on nested simple-laminate constructions based on ideas from [3], in particular, a convex integration argument in the spirit of [5].

Extensions of this model for layered bicomposites include a generalization to the three-dimensional situation, adding more active slip systems in the softer phase, and dropping the assumption of rigid elasticity by accounting for non-trivial elastic energies. In the next steps, we plan to replace the rigid component in the model by one with a rotated slip system, and to account for slip band-grain boundary interaction by incorporating a regularization term in the form of a suitable grain

boundary energy. Furthermore, by using methods from stochastic homogenization, we seek to analyze polycrystalline materials with non-periodically arranged grains and random texture.

References

[1] F. Christowiak, C. Kreisbeck, *Homogenization of layered materials with rigid components in single-slip finite plasticity*, in preparation.

[2] S. Conti, *Relaxation of single-slip single-crystal plasticity with linear hardening*, In: Multiscale Materials Modeling, P. Gumbsch (ed.), Fraunhofer IRB, Freiburg, 2006, 30–35.

[3] S. Conti, F. Theil, *Single-slip elastoplastic microstructures*, Arch. Ration. Mech. Anal. **178**(1) (2005), 125–148.

[4] G. Dal Maso, *An introduction to Γ-convergence*, Progress in nonlinear differential equations and their applications, Volume 8, Birkhäuser Boston, 1993.

[5] S. Müller, V. Šverák, *Convex integration with constraints and applications to phase transitions and partial differential equations*, J. Eur. Math. Soc. **1**(4) (1999), 393–422.

[6] D. Raabe, *Computational Materials Science: The Simulation of Materials, Microstructures and Properties*, Wiley-VCH Verlag, 2004.

[7] J. Schröder, K. Hackl, *Plasticity and beyond: Microstructures, crystal-plasticity and phase transitions*, CISM International Centre for Mechanical Sciences **550**, Springer Wien, 2013.

Dislocation mechanism of microstructural changes in ductile single crystals

Khanh Chau Le

(joint work with Christina Günther, Michael Koster, Binh Duong Nguyen)

The present paper considers three problems: (i) martensitic phase transition involving dislocations, (ii) formation of grain boundaries during severe plastic deformations, (iii) formation of shear bands in a single crystal plate under uniaxial compression. All problems turn out to be non-convex variational problems of energy minimization that will be solved within the continuum dislocation theory (CDT) proposed in [1]. In the first problem it will be shown that the co-existence of phases having piecewise constant plastic slip in laminates is possible for the two-well free energy density. The jumps of the plastic slip across the phase interfaces determine the surface dislocation densities at those incoherent boundaries. The number of phase interfaces should be determined by comparing the energy of dislocation arrays and the relaxed energy minimized among uniform plastic slips. The stress-strain curve shows some load-drop at the onset of phase transition and the elastic behavior of the second phase when the phase transition is finished followed by perfectly plastic behavior afterwards. The work hardening behavior is also possible if the side boundaries of the strip are clamped forcing the dislocations to pile up near these boundaries. In the second problem we interpret the grain boundary as surfaces of weak discontinuity in placement but strong discontinuity in plastic slip. The set of governing equations and jump conditions are derived for the energy minimizers admitting such surfaces of discontinuity from the variational principle. By constructing energy minimizing sequences having piecewise constant plastic and elastic deformation for ductile single crystals deforming in

plane strain simple shear, it is shown that the formation of lamellae structure with grain boundaries is energetically preferable. The number of lamellae is estimated by minimizing the energy of grain boundaries plus the energy of boundary layers [3]. We compute also the thickness and the energy of grain boundary as functions of the misorientation angle and show that the dislocations concentrated in these grain boundaries do not produce long-range stress field [4]. In the third problem of formation of shear bands in a single crystal plate under uniaxial compression the uniform states are not rank-one connected, so dislocations and grain boundaries should adapt to the elastic strains chosen from the homogeneous states in a smart way to satisfy the compatibility condition and, at the same time, to minimize the energy. It turns out that the whole set of jump conditions is needed to determine the orientation of grains (which are misoriented with respect to the slip direction), the plastic slips, and the elastic rotations [3].

References

[1] K.C. Le, C. Günther, *Nonlinear continuum dislocation theory revisited*, International Journal of Plasticity **53** (2014), 164–178.

[2] K.C. Le, C. Günther, *Martensitic phase transition involving dislocations*, Journal of the Mechanics and Physics of Solids **79** (2015), 67–79.

[3] M. Koster, K.C. Le, B.D. Nguyen, *Formation of grain boundaries in ductile single crystals at finite plastic deformations*, International Journal of Plasticity **69** (2015), 134–151.

[4] M. Koster, K.C. Le, *Formation of grains and dislocation structure of geometrically necessary boundaries*, Material Science and Engineering A **643** (2016), 12–16.

Propagation of Complex Fracture

ROBERT LIPTON

Dynamic brittle fracture is a multiscale phenomenon operating across a wide range of length and time scales. It presents a challenging problem for continuum modeling because of the extremes of strain and strain-rate experienced by the material near a crack tip and because of the inherent instabilities such as branching that characterize many applications. In this research a nonlocal and nonconvex model is formulated for calculating the deformation inside a cracking body. Here the nonconvex potential is useful for describing both elastic deformation and material softening. We work within the small deformation nonlocal setting and the strains are calculated as difference quotients. The constitutive relation is given by a nonlocal cohesive law relating force to strain. We find that nonconvexity within nonlocal mechanics provides a mechanism for crack nucleation and growth through material instability. At each instant of the evolution a process zone is identified where strains lie above a threshold value beyond which the force between points begins to decrease. Perturbation analysis shows that jump discontinuities within the process zone can become unstable and grow. We derive an explicit inequality that shows that the size of the process zone is controlled by the ratio given by the length scale of nonlocal interaction divided by the characteristic dimension of the sample. The process zone is shown to concentrate on a set of zero volume in the

limit where the length scale of nonlocal interaction vanishes with respect to the size of the domain. In this limit the dynamic evolution is seen to have bounded linear elastic energy and Griffith surface energy. The limit dynamics corresponds to the simultaneous evolution of linear elastic displacement and the fracture set across which the displacement is discontinuous. We note that components of the approach developed here can be applied to identify limits of dynamics associated with other energies that Γ- converge to the Griffith fracture energy.

References

[1] R. Lipton, *Cohesive dynamics and brittle fracture*, Journal of Elasticity (2015), DOI:10.1007/s10659-015-9564-z.
[2] R. Lipton, *Dynamic brittle fracture as a small horizon limit of peridynamics*, Journal of Elasticity **117** (2014), 21–50.
[3] R. Lipton, S. Silling, and R .Lehoucq, *Complex fracture nucleation and evolution with nonlocal elastodynamics*, Feb. 2, 2016, arXiv:1602.00247.

Application of crystal plasticity in the field of microelectronics

Felix Meier
(joint work with Ewald Werner)

Growing demands on performance and durability of integrated circuits require an understanding of typical failure mechanisms which are triggered by cyclic thermo-mechanical loading. The schematic cross section in figure 1 illustrates the layered structure of a section of an integrated circuit. The conductor paths are constituted of polycrystalline single-phase aluminium and are surrounded by an interlayer dielectric (ILD) of silicon oxide. The substrate consists of silicon and the metallization plate again of aluminium. During operation the current flow in the conductor paths leads to cyclic thermal loads on the device. As a result of the different thermal expansion behaviour of the involved materials, the thermal loads lead to mechanical loads which, in turn, cause plastic deformation. Typical types of damage are surface roughening of the metallization plate and either lateral or vertical crack initiation within the ILD. The crack is subsequently filled with aluminium and causes an electrical short destroying the functionality of the device.

Via simulation we investigated the influence of the Al-microstructure on the probability of crack initiation by utilizing a crystal plasticity material model which bases on the code *DAMASK* (developed at the Max-Planck-Institut für Eisenforschung, Düsseldorf) and was enriched with respect to thermal expansion and temperature and grain size dependency of the mechanical properties. In crystal plasticity it is assumed that dislocation glide in slip systems facilitates plastic flow. Therefore, the stress acting on a grain is projected into the slip systems using Schmid's law. After that, for each slip system the temperature dependent shear rate and the temperature dependent critical shear stress rate (defines at which stress level slipping starts to occur) are calculated thereby taking into account the mutual interactions of the slip systems' activities. The critical shear
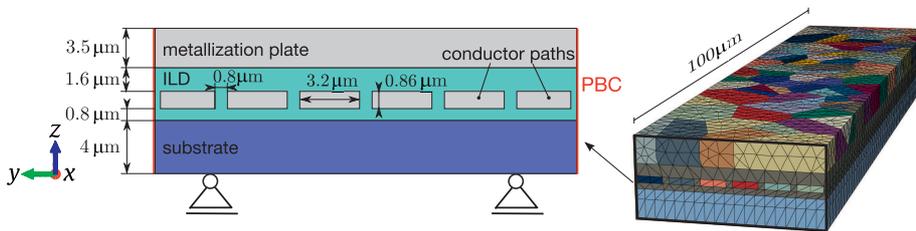
FIGURE 1. Left: Schematic cross section of the simulation model with its dimensions and boundary conditions. Right: Exemplary simulation model with a specific predefined microstructure (each grain is coloured differently).

stress is not only defined by the mechanical hardening but also by the thermal hardening or softening depending on the evolution of temperature. Furthermore we assume isotropic thermal expansion and decompose the overall deformation gradient multiplicatively into thermal, elastic and plastic parts. Finally, the influence of the grain size is taken into account by means of the Hall-Petch-relation whose parameters were determined in micropillar-compression tests [1]. A more precise insight into the material model is presented in [2, 3] and concerning fundamental principles of crystal plasticity modelling the authors refer to the literature [4, 5, 6, 7].

The remainder of the simulation model are treated as purely elastic. The bottom surface is fixed in z-direction and a periodic boundary condition is applied to the left and right faces in order to mimic an infinite model width. The thermal boundary conditions, see fig 2, are applied thus that the same spatial and temporal temperature distribution is achieved as observed by experiments [8, 9, 10]. The simulation starts with a homogeneous temperature distribution at 498 K, which is the fabrication temperature of the conductor paths. After an one-time cool down to 398 K ten load cycles are applied with a logarithmic sawtooth temperature evolution. The highest temperature fluctuation occurs within the conductor paths at $x < 50\,\mu$m.

In the context of a parameter study the mean grain size of the metallization plate grains was varied in a range of $2 - 15\,\mu$m. Furthermore, three different types of grain orientations were distinguished for both the metallization plate and the conductor paths: no texture (grain orientation is random), [111]-texture ([111] || z-axis) which is the predominant orientation in a real device [11] and [001]-texture ([001] || z-axis). Our results reveal that the maximum principal stress within the ILD can be reduced by increasing the mean grain size of the metallization plate grains and can be even halved by resolving the [111]-texture of the conductor path grains. It became apparent that the [111]-texture subjects the ILD with the highest possible stress level. As reported in [2], a multilayer construction of the conductor paths enforces smaller grains and thereby conduces to a life time extension by reducing the stress level within the ILD. The surface roughening of
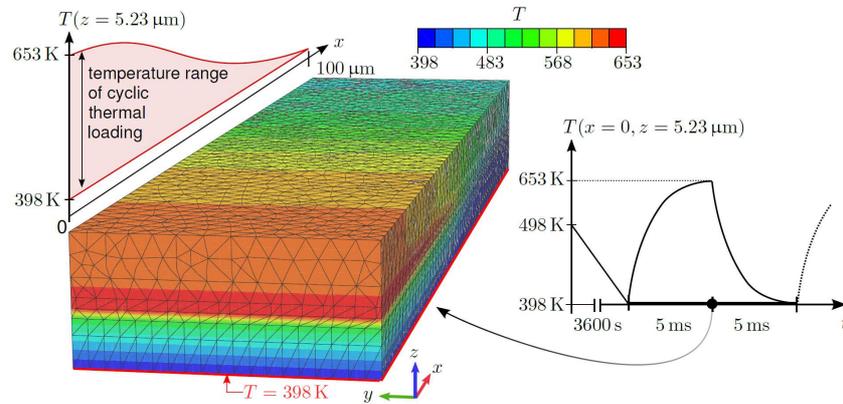
FIGURE 2.   The right diagram shows the temperature history
within the conductor paths at $x = 0$. After an initial homogeneous
cooling from 498K to 398K, 10 inhomogeneous thermal load cycles
are applied reaching a maximum temperature of 653K. The left
image illustrates the temperature distribution after heating.

the metallization plate can also be reduced by resolving the [111]-texture and by
increasing the grain size in the domain of the highest temperature fluctuation [3].

REFERENCES

[1] T. Smorodin, J. Wilde, P. Nelle, E. Lilleodden, M. Stecher, *Modeling of DMOS subjected
    to fast temperature cycle stress and improvement by a novel metallization concept*, IEEE
    International Reliability Physics Symposium Proceedings (2008), 689–690.
[2] F. Meier, C. Schwarz, E. Werner, *Crystal-plasticity based thermo-mechanical modeling of
    Al-components in integrated circuits*, Computational Materials Science **94** (2014), 122–131.
[3] E. Werner, R. Wesenjak, A. Fillafer, F. Meier, C. Krempaszky, *Microstructure-based mod-
    elling of multiphase materials and complex structures*, Continuum Mechanics and Thermo-
    dynamics (2015), 1–22.
[4] J. Clayton, *Dynamic plasticity and fracture in high density polycrystals: constitutive mod-
    eling and numerical simulation*, Journal of the Mechanics and Physics of Solids **53** (2005),
    261–301.
[5] S. Kalidindi, C. Bronkhorst, L. Anand, *Crystallographic texture evolution in bulk deforma-
    tion processing of FCC metals*, Journal of the Mechanics and Physics of Solids **40** (1992),
    537–569.
[6] F. Roters, P. Eisenlohr, T. R. Bieler, D. Raabe, *Crystal plasticity finite element methods:
    in materials science and engineering*, Wiley-VCH, Weinheim, 2010.
[7] F. Roters, P. Eisenlohr, L. Hantcherli, D. Tjahjanto,T. Bieler, D. Raabe, *Overview of
    constitutive laws, kinematics, homogenization and multiscale methods in crystal plastic-
    ity finite-element modeling: Theory, experiments, applications*, Acta Materialia **58** (2010),
    1152–1211.

[8] W. Kanert, R. Pufall, O. Wittler, R. Dudek. M. Bouazza, *Modelling of metal degradation in power devices under active cycling conditions*, IEEE Multi-Physics Simulation and Experiments (2011), 1/6–6/6.

[9] T. Smorodin, J. Wilde, P. Alpern, M. Stecher, *A Temperature-Gradient-Induced Failure Mechanism in Metallization Under Fast Thermal Cycling*, IEEE Transactions on Device and Materials Reliability **8** (2008), 590–599.

[10] M. Glavanovics, H. Köck, V. Košel, T. Smorodin, *Flexible active cycle stress testing of smart power switches*, Microelectronics Reliability **47** (2007), 1790–1794.

[11] T. Smorodin, *Modellierung von Schädigungsmechanismen in Metallisierungsschichten unter schneller Temperaturwechselbelastung*, Der Andere Verlag, Tönning, 2008.

Meso-scale continua for moving interfaces in fluids and solids: open problems

Sinisa Mesarovic

The following open questions are disussed on two example probems:

- Diffuse (mesoscale phase field) vs. sharp interface,
- Mathematical and physical arguments for diffuseness,
- Phase field parameter identification,
- Continua with mixing (ordered and disordered),
- Connection between 3D continuum 2D continuum (sharp interface),
- Uniqueness and stability of phase field solutions.

The example problems described are:
(a) Capillary flow (phase field), and, (b) diffusional creep of polycrystals (sharp interface).

(a) We define the capillary flow as the flow of at least two fluid components driven or controlled by capillary forces. These forces are exerted at the triple line where the two fluids meet the solid boundary. Consequently, the motion of the triple line is the key component in any capillary flow model. In the phase-field model the triple line moves by surface diffusion mechanism, thus allowing for the no-slip boundary condition without the stress singularities. Moreover, the phase field framework is uniquely suited for the modeling of topological discontinuities which often arise during capillary flow. The numerical method of choice is the finite element method, which: (i) allows simple implementation of the diffusive boundary conditions, (ii) is suitable for modeling complex geometries, and, (iii) allows variable mesh density needed for the phase field model.

We consider two types of phase-field models, the compositionally compressible (CC) and the incompressible model (IC) with their corresponding diffusive triple line conditions. We show that the latter represents the approximation to the former, with typically negligible error. We discover that the CC model, applied to the fluids of dissimilar mass densities, exhibits a computational instability at the triple line, as well as a very slow convergence. We show that the IC model perfectly represents the analytic equilibria. To benchmark the kinetics IC model against experiments, we

develop the parameter identification procedure and show that the triple line kinetics can be well represented by the IC models diffusive boundary condition. Finally, we investigate the effects of the phase-field diffusional mobility parameter on the kinetics of the wetting process.

(b) Diffusional creep is characterized by growth/disappearance of lattice planes at the crystal boundaries which serve as sources/sinks of vacancies, and by diffusion of vacancies. The lattice continuum theory developed here represents the natural and intuitive framework for analysis of diffusion in crystals and lattice growth/loss at the boundaries. The formulation includes the definition of the Lagrangean reference configuration for the newly created lattice, the transport theorem, and the definition of the creep rate tensor as constant within a crystal and related the normal diffusional flux at the boundaries.

The governing equations for Nabarro-Herring creep are developed with coupled diffusion and elasticity. Both, the bulk diffusional dissipation and the boundary dissipation accompanying vacancy nucleation and absorption, are considered, but the latter is found to be negligible. For periodic arrangements of grains, diffusion formally decouples from elasticity but at the cost of a complicated boundary condition. The equilibrium of deviatorically stressed polycrystals is impossible without inclusion of interface energies. The secondary creep rate estimates correspond to the standard Nabarro-Herring model, and the volumetric creep is small. The main features of primary creep are qualitatively understood and some avenues of research are suggested for the transition from secondary to tertiary creep.

Size-dependent energy in mesoscale dislocation-based continua

Sinisa Mesarovic

In the light of recent progress in coarsening the discrete dislocation mechanics, we consider two questions relevant for the development of a mesoscale, size-dependent plasticity:

(i) Can the phenomenological expression for size-dependent energy, as quadratic form of Nye's dislocation density tensor, be justified from the point of view of dislocation mechanics and under what conditions?

(ii) How can physical or phenomenological expressions for size-dependent energy be computed from dislocation mechanics in the general case of elastically anisotropic crystal?

The analysis based on material and slip system symmetries implies the negative answer to the first question. However, the coarsening method developed in response to the second question, and based on the physical interpretation of the size-dependent energy as the coarsening error in dislocation interaction energy, introduces additional symmetries. The result is that the equivalence between the phenomenological and the physical expressions is possible, but only if the multiplicity of characteristic lengths associated with different slip systems, is sacrificed.

Finally, we discuss the consequences of the assumption that a single length scale governs the plasticity of a crystal, and note that the plastic dissipation at interfaces has a strong dependence on the length scale embedded in the energy expression.

Relaxation of a rate-independent phase transformation model for the evolution of microstructure
Alexander Mielke

Microstructures in macroscopic and mesoscopic material models are often described on the basis of the strain tensor and some internal variables such as phase indicators, magnetization, plastic tensor, or hardening variables. In most cases, the stored-energy density depends only on the point values of these variables and thus defines a material model without any length scale. Thus, even steady states, which occur as minimizers of the energy, may develop microstructures on arbitrary fine scales if the energy density lacks quasi- or polyconvexity. Despite of the missing compactness, for these static problems a far-reaching theory for describing microstructures was developed, starting from [1].

The modeling of the temporal behavior of such microstructures under changing mechanical or thermal loading is significantly more difficult. The variational approach which is based on an energy functional and a dissipation potential or distance allows for special methods. General theory for evolutionary Γ-convergence are available, see [4] for a survey. However, most of these methods need some some type of compactness which is not available for material models without internal length scale. For the special case of rate-independent systems, which do not have an intrinsic time scale and hence are sufficiently close to static problems, a major step forward was done using incremental minimization problems. The formation of microstructure was detected and discussed in [9, 2].

The approach based on incremental minimization problems leads to the concept of *energetic solutions* for rate-independent systems $(\mathcal{Q}, \mathcal{E}, \mathcal{D})$, see [5] for a comprehensive treatment. Here $\mathcal{Q}$ is the state space, $\mathcal{E} : [0,T] \times \mathcal{Q} \to \mathbb{R}$ is the energy functional, and $\mathcal{D} : \mathcal{Q} \times \mathcal{Q} \to [0, \infty]$ is the dissipation distance. For initial states $q_0 \in \mathcal{Q}$, we consider the

---

Approximate Incremental Minimization Problem

(AIMP) $\begin{cases} \text{for } j = 1, ..., J \text{ find } q_j \in \mathcal{Q} \text{ with} \\ \mathcal{E}(j\tau, q_j) + \mathcal{D}(q_{j-1}, q_j) \leq \varepsilon\tau + \mathcal{E}(j\tau, \widehat{q}) + \mathcal{D}(q_{j-1}, \widehat{q}) \text{ for all } q \in \mathcal{Q}, \end{cases}$

where $\tau = T/J > 0$ is the time step and $\varepsilon \geq 0$ an accuracy level.

For $\varepsilon > 0$ approximate minimizers always exist, however the solutions q_j^ε develop microstructure for $\varepsilon \to 0$. Defining the piecewise constant interpolants $q_{\tau,\varepsilon} : [0,T] \to \mathcal{Q}$ via $q_{\tau,\varepsilon}(t) = q_{j-1}^\varepsilon$ for $t \in [(j-1)\tau, j\tau[$ the major mathematical task in *evolutionary relaxation* is

- to establish convergence of a suitable subsequence for $\tau_n,\ \varepsilon_n \to 0$,
- to identify a limit $q : [0,T] \to \mathcal{Q}$, and
- to determine an evolution equation for all such limits q.

The recent research in [3] is a continuation of previous work on a simple but non-trivial two-phase model without without internal length scale, and hence without compactness. The results are threefold: introduced in [6, 8] with the following new results: (i) the existence theory for the separately relaxed two-phase model introduced in [6, 8] is generalized, (ii) a numerical convergence result for space-time discretizations is provided, and (iii) the evolutionary relaxation of the rate-independent "pure-state model" is shown to lead exactly to the model studied in (i).

The pure-state model $(\mathbf{U}\times\mathcal{Z}^{\mathrm{pure}},\mathcal{E},\mathcal{D})$ is characterized that the phase indicator $z : \Omega \to \mathbb{R}$ only takes two values, viz. $\mathcal{Z}^{\mathrm{pure}} = \left\{\, z \in L^2(\Omega)\,\middle|\, z(x) \in \{1,0\}\ \text{a.e.}\,\right\}$, whereas the relaxed model $(\mathbf{U}\times\mathcal{Z},\mathcal{E},\mathcal{D})$ is defined on the weak closure of $\mathcal{Z}^{\mathrm{pure}}$, namely $\mathcal{Z} = \left\{\, z \in L^2(\Omega)\,\middle|\, z(x) \in [0,1]\ \text{a.e.}\,\right\}$. The new observation in [3] is that the method of *mutual recovery sequences*, which was introduced in [7] (cf. also [5]), can be employed effectively also in cases without compactness. For a given sequence $q^k = (u^k, z^k) \in \mathbf{U}\times\mathcal{Z}^{\mathrm{pure}}$ with $q^k \rightharpoonup q = (u,\theta)$ in $\mathbf{U}\times\mathcal{Z}$ and a comparison state $\widehat{q} = (\widehat{u},\widehat{\theta}) \in \mathbf{U}\times\mathcal{Z}$, a sequence $(\widehat{q}^k)_{k\in\mathbb{N}}$ is called a mutual recovery sequence, if $\widehat{q}^k \rightharpoonup \widehat{q}$ and

$$\limsup_{k\to\infty}\left(\mathcal{E}(t,\widehat{q}^k) + \mathcal{D}(q^k,\widehat{q}^k) - \mathcal{E}(t,q^k)\right) \le \mathcal{E}(t,\widehat{q}) + \mathcal{D}(q,\widehat{q}) - \mathcal{E}(t,q).$$

The point is that here that $\widehat{q}^k$ has to contain a suitable microstructure adapted to q^k such that in the above term the special sum of three terms behaves well. This is typically realized by asking

$$(1)\qquad \mathcal{D}(q,\widehat{q}) \;=\; \lim_{k\to\infty}\mathcal{D}(q^k,\widehat{q}^k)\quad\text{and}$$

$$(2)\qquad \mathcal{E}(t,\widehat{q}) - \mathcal{E}(t,q) \ge \limsup_{k\to\infty}\left(\mathcal{E}(t,\widehat{q}^k) - \mathcal{E}(t,q^k)\right).$$

Using such mutual recovery sequences, it is possible to show the full evolutionary relaxation result: for any approximate solutions $q_{\tau,\varepsilon}$ for $(\mathbf{U}\times\mathcal{Z}^{\mathrm{pure}},\mathcal{E},\mathcal{D})$ obtained via (AIMP) there exists a subsequence q_{τ_k,ε_k} that converges to a limit $q = (u,z) : [0,T] \to \mathbf{U}\times\mathcal{Z}$ which is an energetic solution of the separately relaxed rate-independent system $(\mathbf{U}\times\mathcal{Z},\mathcal{E},\mathcal{D})$. The proof of (i) and (ii) relies on a specific construction for the phase indicator, namely $\widehat{z}^k = \widehat{z} + g(x)(z^k - z)$. The choice of g is crucial for obtaining (1) while keeping $\widehat{z}^k \in \mathcal{Z}$. Then (2) follows by using the quadratic nature of $\mathcal{E}(t,\cdot,\cdot)$ and the theory of H-measures, see [10].

For the evolutionary relaxation result (iii) the construction of $\widehat{z}^k$ is more difficult, since we need $\widehat{z}^k \in \mathcal{Z}^{\mathrm{pure}}$. Here the construction is achieved by introducing suitable laminates on a much finer spatial scale than the microstructure in z^k. Using this scale separation, it is possible to calculate the generates H-measure and obtain (1) and (2) as well.

REFERENCES

[1] J. M. Ball, R. D. James, *Fine phase mixtures as minimizers of energy*, Arch. Rational Mechanics Analysis **100**(1) (1987), 13–52.

[2] C. Carstensen, K. Hackl, A. Mielke, *Non–convex potentials and microstructures in finite–strain plasticity*, Proc. Royal Soc. London Ser. A **458**(2018) (2002), 299–317.

[3] S. Heinz, A. Mielke, *Existence, numerical convergence, and evolutionary relaxation for a rate-independent phase-transformation model*, Phil. Trans. Royal Soc. A **374** (2016) in print (WIAS Preprint 2163).

[4] A. Mielke, *On evolutionary Γ-convergence for gradient systems (Ch. 3)*, In: Macroscopic and Large Scale Phenomena: Coarse Graining, Mean Field Limits and Ergodicity, A. Muntean, J. Rademacher, A. Zagaris (eds.), LAMM Vol. 3, Springer (2016), 187–249.

[5] A. Mielke, T. Roubíček, *Rate-Independent Systems: Theory and Application*, Applied Mathematical Sciences, Vol. 193, Springer-Verlag New York (2015).

[6] A. Mielke, F. Theil, *A mathematical model for rate-independent phase transformations with hysteresis*, In: Proc. Workshop Models of Continuum Mechanics in Analysis and Engineering, H.-D. Alber, R. Balean, R. Farwig (eds.), Shaker (1999), 117–129.

[7] A. Mielke, T. Roubíček, U. Stefanelli, *Γ-limits and relaxations for rate-independent evolutionary problems*, Calc. Var. Part. Diff. Eqns. **31** (2008), 387–416.

[8] A. Mielke, F. Theil, V. I. Levitas, *A variational formulation of rate–independent phase transformations using an extremum principle*, Arch. Rational Mechanics Analysis **162** (2002), 137–177.

[9] M. Ortiz, E. Repetto, *Nonconvex energy minimization and dislocation structures in ductile single crystals*, J. Mech. Phys. Solids **47**(2) (1999), 397–462.

[10] L. Tartar, *H-measures, a new approach for studying homogenisation, oscillations and concentration effects in partial differential equations*, Proc. Roy. Soc. Edinburgh Sect. A **115**(3-4) (1990), 193–230.

Mathematical multiscale analysis in continuum mechanics
STEFAN NEUKAMM

In my presentation I discussed a selection of mathematical methods for the analysis of macroscopic properties in continuum systems with multiple scales; in particular, homogenization methods for linearly elastic composites with periodic and random microstructure, and aspects of the notion of Γ-convergence.

To motivate general ideas, imagine a model (M_ε) that resolves properties on two (or more) scales and which describes a "quantity of interest", say a state variable u_ε. The index ε stands for a small scaling parameter (or a collection of scaling parameters) that has the meaning of a ratio between the micro- and macroscale in the model. Models of that type often show an *effective behavior*, i.e. the quantity of interest u_ε follows (up to small microscopic fluctuations) a "law" that can be stated on the level of macroscopic quantities in a consistent way, while the law itself depends (possibly in a complex way) on the microstructural details of the model. The prospect of multiscale analysis is to gain a mathematical understanding of this interesting phenomena. A natural approach in mathematics is to study the limit $\varepsilon \downarrow 0$, which corresponds to a separation of scales. Various questions on

different levels can be posed. From the viewpoint of mathematical analysis the most fundamental ones are:

- Can we prove convergence of u_ε towards some quantity u_0?
- Can we identify an effective model (M_0) that characterizes u_0?
- Can we understand the relation between microstuctural properties and the effective model (M_0)?

I. A classical example is **homogenization** of partial differential equations. E.g. consider the boundary value problem of linear elastostatics

(1)
$$-D \cdot (\mathbb{C}(\tfrac{\cdot}{\varepsilon})Du_\varepsilon) = f \qquad \text{in } \Omega \subset \mathbb{R}^d$$
$$u_\varepsilon = g \qquad \text{on } \partial\Omega,$$

where $\mathbb{C} = \mathbb{C}(x)$, $x \in \mathbb{R}^d$, denotes a tensor field describing a periodic linearly elastic composite material. Obviously, this model has two length scales: A lengthscale L given by the dimension of the domain Ω and another one, say $\ell \sim \varepsilon L$, given by the period of the composite. A classical result from homogenization theory (e.g. see [1]) shows that the solution u_ε weakly converges in H^1 towards a desplacement field u_0, which turns out to be the *unique* solution to the *homogenized equation*

(2)
$$-D \cdot (\mathbb{C}_{\text{hom}}Du_0) = f \qquad \text{in } \Omega \subset \mathbb{R}^d$$
$$u_0 = g \qquad \text{on } \partial\Omega.$$

Here, the homogenized tensor $\mathbb{C}_{\text{hom}}$ is constant in space and thus describes a homogeneous material. It is characterized by the so called *homogenization formula*: For all displacement gradients F we have

(3)
$$\mathbb{C}_{\text{hom}}F = \int_\square \mathbb{C}(F + D\phi_F),$$

where $\square$ denotes the reference cell of periodicity (associated with the periodic composite), and ϕ_F denotes a corrector, which is defined as the periodic displacement field that solves the *periodic corrector equation*

$$-D \cdot \mathbb{C}(F + D\phi_F) \qquad \text{in } \square \text{ with periodic boundary conditions.}$$

The corrector ϕ_F encodes the spatial fluctuations in the displacement field that are induced by the material's heterogeneity. It allows to predict microscopic details of u_ε by means of a **two-scale expansion**:

$$u_\varepsilon(x) \approx \tilde{u}_\varepsilon := u_0(x) + \varepsilon\phi_j^\alpha(\tfrac{x}{\varepsilon})\partial_\alpha u_{0,j}(x) \qquad \text{away from the boundary } \partial\Omega.$$

This can be easily justified by formal asymptotics. In [1] this expansion is made rigorous and quantitative; we recall this result in form of the following estimate (which only holds away from the boundary):

$$\int |u_\varepsilon - \tilde{u}_\varepsilon|^2 + |Du_\varepsilon - D\tilde{u}_\varepsilon|^2 \lesssim \varepsilon^2 \left(\int (|\phi(\tfrac{\cdot}{\varepsilon})|^2 + |\sigma(\tfrac{\cdot}{\varepsilon})|^2)|D^2u_0|^2 \right),$$

see e.g. [2] for details. Under additional regularity assumptions on the geometry of the domain, boundary data and forcing, the right-hand side scales as ε^2, which

is optimal. The behavior close to the boundary is subtle, see [3] for a recent contribution.

II. In **stochastic homogenization** one considers (1) with a tensor field $\mathbb{C}$ that is random (more precisely a stationary and ergodic tensor field) and thus describes material with random microstructure. An intuitive example for a random material is the following: Tile space into square fields and in each field randomly pick a material that occupies this field. Do that in an independent and identically distributed way. The result, the "random checkerboard material", is a stationary random field with finite length of correlation. In [7] it is shown that homogenization also occurs in the random (stationary & ergodic) case and that the limit is again discribed by the deterministic and constant-coefficient equation (3). We also have a homogenization formula, which takes the asymptotic form

$$(4) \qquad \mathbb{C}_{\text{hom}} F = \lim_{L \to \infty} \frac{1}{|\square_L|} \int_{\square_L} \mathbb{C}(F + D\phi_F),$$

where $\square_L$ denotes a box of side length L. Due to the limit $L \uparrow \infty$, (4) requires approximation by means of computable quantities. A natural approximation is the following "periodic representative volume element"-type construction: For $L \gg 1$ sample a material on the box $\square_L$ and compute a periodic proxy $\mathbb{C}_L$ by means of the periodic homogenization formula. Note that $\mathbb{C}_L$ is a random tensor, which fluctuates around its average $< \mathbb{C}_L >$, where $< \cdot >$ denotes the ensemble average. In order to decrease these fluctuations repeat the procedure N-times and take the empirical average. This yields the (random) tensor $\mathbb{C}_{N,L} := \frac{1}{N} \sum_{i=1}^{N} \mathbb{C}_{N,L}^i$. In [4] we prove in a simplified setting (discrete, scalar elliptic equation, i. i. d. statistics) the estimate

$$\left\langle |\mathbb{C}_{\text{hom}} - \mathbb{C}_{\text{hom},L,N}|^2 \right\rangle^{\frac{1}{2}} \le C \left(\frac{1}{\sqrt{N}} L^{-\frac{d}{2}} + L^{-d} \ln^d L \right),$$

by combining a concentration inequality for the ensemble with elliptic regularity theory. In [2] we extend substantial methods to continuum systems with correlations and prove an optimal estimate for the two-scale expansion in the random case. These results are examples for **quantitative stochastic homogenization** - e.g. see [4, 2, 5, 6] and the references therein for recent developements.

III. The notion of **Γ-convergence** was introduced by De Giorgi in the 70s and is taylor made for minimization problems. It has been applied to various problems e.g. homogenization [8, 9], atomistic-to-continuum modeling [10], singular perturbation [11], derivation of plate theories and its combination with homogenization [12, 13]. Although Γ-convergence is mostly applied to static problems, some extensions to evolution problems have been achieved, see e.g. [14, 15, 16].

References

[1] A. Bensoussan, J.-L. Lions, G. Papanicolaou, *Asymptotic analysis for periodic structures*, AMS Chelsea Publishing, 2011.
[2] A. Gloria, S. Neukamm, F. Otto, *A regularity theory for random elliptic operators*, arXiv:1409.2678

[3] D. Gérard-Varet, N. Masmoudi, *Homogenization and boundary layers*, Acta Math. **209**(1) (2012), 133–178.

[4] A. Gloria, S. Neukamm, F. Otto, *Quantification of ergodicity in stochastic homogenization: optimal bounds via spectral gap on Glauber dynamics*, Invent. Math. **199**(2) (2015), 455–515.

[5] S. Armstrong, T. Kuusi, J.-C. Mourrat, *The additive structure of elliptic homogenization*, arXiv:1602.00512

[6] M. Duerinckx, A. Gloria, F. Otto, *The structure of fluctuations in stochastic homogenization*, arXiv:1602.01717

[7] G. Papanicolaou, S. R. S. Varadhan, *Boundary value problems with rapidly oscillating random coefficients*, Random fields, Vol. I, II (Esztergom, 1979), Colloq. Math. Soc. János Bolyai, vol. 27, North-Holland, 1981.

[8] S. Müller, *Homogenization of nonconvex integral functionals and cellular elastic materials*, Arch. Rat. Anal. Mech. **99** (1987), 189–212.

[9] A. Braides, *Homogenization of some almost periodic coercive functional*, Rend. Accad. Naz. Sci. XL **103** (1985), 313–322.

[10] A. Braides, M.S. Gelli, *From Discrete to Continuum: a Variational Approach*, Lecture Notes. SISSA, Trieste, 2000.

[11] L. Modica, S. Mortola, *Un esempio di Γ-convergenza*. Boll. Un. Mat. Ital. **14-B** (1977), 285–299.

[12] G. Friesecke, R. D. James, S. Müller, *A hierarchy of plate models derived from nonlinear elasticity by Gamma-convergence*, Arch. Rat. Mech. Analysis. **2** (2006), 183–236.

[13] S. Neukamm, I. Velcic, *Derivation of a Homogenized Von-Kármán Plate Theory from 3d Nonlinear Elasticity*. Mathematical Models and Methods in Applied Sciences **23**(14) (2013), 2701–2748.

[14] S. Serfaty, *Gamma-convergence of gradient flows on Hilbert and metric spaces and applications*, Discrete Contin. Dyn. Syst. **31**(4), 1427–1451

[15] A. Mielke, T. Roubícek, *Rate-Independent Systems: Theory and Application*, Applied Mathematical Sciences, Volume 193, Springer 2015.

[16] A. Mielke, *On evolutionary Γ-convergence for gradient systems*, Lecture Notes in Appl. Math. Mech., 187–249, Springer 2016.

About an analytical approach to a quasicontinuum method and continuum limits of discrete systems that allow for fracture

Anja Schlömerkemper

(joint work with Mathias Schäffner)

Quasicontinuum methods are computational schemes that are applied to efficiently treat mechanical systems, of which a full atomistic computation is too expensive. This is for instance useful in an elastic material that experiences a crack. One then considers a non-local model close to the crack tip (atomistic region) and a local model away from the crack (continuum region), see [6] and the abstract by D. Kochmann given at this workshop. There are various analytical results on quasicontinuum methods from the numerical point of view, see [2] for a recent overview.

Here we follow a different approach. We aim for understanding the quasicontinuum method as a model that serves as an approximation of a continuum theory. This perspective fits to a broader research topic, in which one wants to verify continuum models as the asymptotic limit of underlying atomistic models and to

understand how to approximate continuum models well by discrete models, cf., e.g., the list of references in [5].

More specifically we present a one-dimensional toy-model of $n+1$ atoms which interact through Lennard-Jones type potentials J_j of finite order, $j = 1, \ldots, K$. See [4] for the case $K = 2$ and [5] for arbitrary but finite K. The chain is fixed at the two ends of the chain and obeys certain conditions on the atoms close to the boundary. Depending on the overall length of the chain, the system behaves elastically or shows cracks. The asymptotic behavior of the energy functional $H_n : L^1(0,1) \to (-\infty, \infty]$,

$$H_n(u) = \begin{cases} \displaystyle\sum_{j=1}^{K} \sum_{i=0}^{n-j} \frac{1}{n} J_j \left(\frac{u^{i+j} - u^i}{j\frac{1}{n}} \right) & \text{if } u \in \mathcal{A}_n(0,1), \\ +\infty & \text{else} \end{cases}$$

of the fully atomistic model is studied by Γ-convergence methods as $n \to \infty$. Here $\mathcal{A}_n(0,1)$ denotes the space of all piecewise affine interpolations of the deformation map u defined on the reference configuration $\frac{1}{n}\mathbb{Z} \cap [0,1]$. The Γ-limit (of zeroth order) is obtained by applying a result of Braides and Gelli [1] and a clever resummation of the energy, which is the crucial new method in this proof. This allows to replace the typical homogenization formula by a Cauchy-Born energy:

$$H_0(u) = \int_0^1 J_{CB}^{**}(u'(x))dx,$$

where J_{CB}^{**} denotes the lower semicontinuous and convex envelope of the Cauchy-Born energy density $J_{CB} = \sum_{j=1}^{K} J_j$.

In addition to the fully atomistic system we study the so-called quasinonlocal quasicontinuum method. This is mimicked by introducing an atomistic region $A(j)$ close to the two ends of the chain and a continuum region $C(j)$ in between, where $j = 1, \ldots, K$. In the continuum region one then (1) replaces all the potentials of the j-interacting neighbors, $1 < j \le K$, by an average of corresponding nearest neighbor interactions and (2) introduces representative atoms in the continuum region. The energy functional can then be written as

$$H_n^{\mathrm{QC}}(u) = \sum_{j=1}^{K} \frac{1}{n} \left\{ \sum_{i \in A(j)} J_j \left(\frac{u^{i+j} - u^i}{j\frac{1}{n}} \right) + \frac{1}{j} \sum_{i \in C(j)} \sum_{s=i}^{i+j-1} J_j \left(\frac{u^{s+1} - u^s}{j\frac{1}{n}} \right) \right\}$$

if u satisfies the required boundary conditions and is an affine function on the given set $\mathcal{T}_n$ of representative atoms. It turns out that the Γ-limit of this functional is equal to the Γ-limit H_0 of the fully atomistic system H_n as $n \to \infty$.

From the mechanical point-of view it is of interest to consider also a Γ-limit of first order, which gives some information on the number and the location of cracks through surface energy (boundary layer energy) contributions. In the case of the fully atomistic chain as well as in the QC model, it turns out that the Γ-limit of first order depends on the boundary condition, i.e., on the given overall length of the chain. As already indicated above, if this length is smaller than a certain

threshold, the system behaves elastically. Above this threshold cracks occur. This is described by different compactness and Γ-convergence results.

In the elastic case, the Γ-limits of first order of the fully atomistic and the QC model coincide. In the case of fracture, the two limits turn out to be different in general, see [4] for $K = 2$ and [3] for arbitrary but finite K.

However, a detailed analysis shows that the minimizers and minimal energies coincide if the chosen set of representative atoms is coarse enough at the interface between the atomistic and the continuum region as well as within the continuum region. More precisely, for $K = 2$ a necessary and sufficient condition is that the minimal distance between two representative atoms is 2 up to the interface [4]. The same result holds for classical Lennard-Jones potentials and arbitrary but finite K, see [3].

References

[1] A. Braides, M. S. Gelli, *The passage from discrete to continuous variational problems: a nonlinear homogenization process*, In: Nonlinear Homogenization and its Applications to Composites, Polycrystals and Smart Materials, NATO Sci. Ser. II Math. Phys. Chem. **170**, Kluwer Acad. Publ., Dordrecht, 2004.

[2] M. Luskin, C. Ortner, *Atomistic-to-continuum coupling*, Acta Numer. **22** (2013), 397–508.

[3] M. Schäffner, *Multiscale analysis of non-convex discrete systems via Γ-convergence*, Dissertation, University of Würzburg, 2015.

[4] M. Schäffner, A. Schlömerkemper, *On a Γ-convergence analysis of a quasicontinuum method*, Multiscale Model. Simul. **13** (2015), 132–172.

[5] M. Schäffner, A. Schlömerkemper, *On Lennard-Jones systems with finite range interactions and their asymptotic analysis*, arXiv:1501.06423.

[6] E. Tadmor, M. Ortiz, R. Phillips, *Quasicontinuum analysis of defects in solids*, Phil. Mag. A **73** (1996), 1529–1563.

The mathematical justification of a consistent, refined beam theory

Patrick Schneider

(joint work with Reinhold Kienzler)

1. Introduction

Classical theories for thin structures like the Euler-Bernoulli beam and the Kirchhoff plate theory were developed by the use of disputable a-priori assumptions already in the 18$^{\text{th}}$ and 19$^{\text{th}}$ century. They are still widely-used in engineering practice since they provide reasonable accuracy, if the structure under consideration is sufficiently thin. Rigorous mathematical justifications for these theories are available which proof them to appear as a limit of the three-dimensional theory of elasticity, if the thickness of the structure tends to zero. Recent results obtained in the present century mostly use the method of Γ-convergence [1, 2], which does not deliver quantitative error estimates directly.

Driven by practical needs of the engineering community, the development of refined theories, i.e., theories for moderately thick structures, or higher precision,

started already in the middle of the 20th century. Nowadays refined theories are still an open topic which is under intensive development. Mathematical justifications for refined theories are missing - even for the most established theories like the Reissner-Mindlin plate theory.

2. The uniform approximation approach

The uniform approximation approach for the a-priori assumption-free derivation of theories for thin structures from the three-dimensional theory of linear elasticity goes back to pioneer treaties of Naghdi [5] and Koiter [4]. Kienzler [3] interprets the approach as a truncation of the elastic energy after a maximum power of a characteristic parameter that describes the relative thickness of the structure. We extend his ideas by truncating the associated dual energy as well, in order to provide a mathematical justification for refined theories by the proof of quantitative error estimates.

By extending a standard result from duality theory (based on Korn's inequality) towards general anisotropy, the square error of an arbitrary displacement field v from the (weak) solution of three-dimensional elasticity can be estimated via the difference $E_{\text{pot}}(v) - E_{\text{dual}}(\mu)$ of the elastic potential and the dual energy of an admissible stress field μ. By using a dimensionless formulation and (abstract) Fourier-series expansions in thickness direction for the displacement field, the potential and dual energy appear as infinite power series in parameters describing the relative thickness of the structure. When truncating both series after a certain power, a finite set of field equations and stress-boundary conditions can be derived from the Euler-Lagrange equations of the potential energy, whereas the dual energy's Euler-Lagrange equations deliver matching displacement-boundary conditions. This generates a hierarchy of theories with regard to the truncation power. By virtue of the mentioned result from duality theory and by factoring out the Euler-Lagrange equations in the difference of energies, the error of the Nth-order approximation theory decreases like the $(N + 1)$th power of the characteristic parameter. Therefore, any solution of an Nth-order theory converges to the three-dimensional solution, if the thickness tends to zero. Furthermore, a considerable gain of accuracy is achieved by increasing the approximation order, which finally proofs the approximation property of the approach.

If smooth solutions are available, one is enabled to reduce the number of unknown displacement coefficients in a certain theory by successive elimination, cf. [7]. This leads to the classical theories for thin structures for first-order approximations and to new refined theories for higher-order approximations.

We already applied the approach for the derivation of a refined monoclinic plate theory, cf. [11], which turns out to be equivalent to the Reissner-Mindlin theory for the special case of an isotropic material. For a comparison to other established higher-order theories we refer to [8].

3. Refined beam theory

In the talk we illustrated the approach by deriving theories for an isotropic, linear elastic quasi one-dimensional structure (length l) with constant rectangular cross-section (width $b \ll l$, height $h \ll l$). The error of the Nth-order approximative theory's solution v_N from the (exact) solution of three-dimensional elasticity u decreases like

$$k \, \|v_N - u\|_X^2 \leq O\left(\max\left\{ \frac{b}{\sqrt{12}l}, \frac{h}{\sqrt{12}l} \right\}^{2(N+1)} \right),$$

where k is a fixed constant.

We proof that the problem decouples into four independent subproblems (a rod-, a shaft- and two beam-problems with orthogonal loading directions) for the arbitrary three-dimensional load case of an one-dimensional isotropic structure. Subproblems are identified by decomposing the prescribed boundary displacement, traction and volume-force into even and odd parts with respect to the axis of the cross-section that is assumed to be two-fold symmetric. Furthermore, we show how the coupling of the subproblems can be derived directly from the sparsity scheme of the stiffness tensor for an arbitrary anisotropic (linear elastic) material. For details we refer to [9].

The first-order approximation of the beam problem (restricted to loads in one thickness direction) results in the Euler-Bernoulli beam theory (with the known boundary conditions) after pseudo reduction. This is not surprising with regard to other results from literature derived by the use of Γ-convergence. However, the classical a-priori assumptions of the theory drop out as a-posteriori results of the pseudo-reduction procedure, so that an a-priori assumption-free derivation of the theory (originated by the truncation of energies alone) is provided.

The second-order beam theory comprises three in general independent load resultants after pseudo reduction. Only in the absence of volume loads, the load resultants become linear independent and can be expressed solely by the classical line load q. This means, the jointly treatment of volume load and traction via one overall load resultant q (which is the common practice in the field of refined theories) will result in a loss of accuracy in general, i.e., the rate of convergence of the second-order consistent theories is not achieved. Only if the volume force is set to zero, i.e., by negligence of dead-weight, the Timoshenko beam theory is obtained as the second-order consistent approximation, if the shear correction factor in this theory is chosen as

$$K = \underbrace{\frac{3}{20} \frac{5\nu + 8}{1 + \nu}}_{\text{Olsson, [6]}} - \beta^2 \frac{\nu}{1 + \nu} \left[\frac{1}{4} + \frac{\beta^2}{\beta^2 + 5} \frac{\nu}{1 + \nu} \right],$$

where $\beta = \frac{b}{h}$ denotes the cross-section aspect ratio and ν denotes Poisson's ratio. Indeed the limit value for $\beta = 0$ (disc-like beam) is a known shear-correction factor attributed to Olsson, cf. [6]. The factor for $\beta \neq 0$ is not known from literature to our best knowledge. It turns negative for usual values of ν and increasing β, i.e., for

plate-like beams. (As a rule of thumb, a beam is considered plate-like, if $\beta > 2$.) Note that by the classical theories one-dimensionally loaded plates are indeed stiffer than beams with identical resulting overall load q. Therefore, the correction factor covers weakening from shear deformations as well as stiffening effects for plate-like beams, rendering the term "shear correction factor" misleading. It has to be noted, again, that the uniform second-order approach does not introduce any correction factors nor any others a-priori assumptions beside the truncation of energies - the shear correction factor is derived by a vis-a-vis comparison of the resulting ordinary differential field equation with Timoshenko's equation.

Peer-reviewed papers with the presented results are in preparation. In the meantime, we refer the interested reader to [10].

REFERENCES

[1] G. Friesecke, R. D. James, S. Müller, *A theorem on geometric rigidity and the derivation of nonlinear plate theory from three-dimensional elasticity*, Communications on Pure and Applied Mathematics **55**(11) (2002), 1461–1506.

[2] G. Friesecke, S. Müller, R. D. James, *Rigorous derivation of nonlinear plate theory and geometric rigidity*, Comptes Rendus Mathematique **334**(2) (2002), 173–178.

[3] R. Kienzler, *On consistent plate theories*, Archive of Applied Mechanics **72** (2002), 229–247.

[4] W. Koiter, *On the mathematical foundation of shell theory*, In: Proc. Int. Congr. of Mathematics, Nice, Volume 3 (1970), 123–130.

[5] P. M. Naghdi, *Foundations of elastic shell theory*, In: Progress in Solid Mechanics, I. Sneddon, R. Hill (eds.), Volume 4, North-Holland, Amsterdam (1963), 1–90.

[6] R. G. Olsson, *Zur Berechnung der Frequenz der Transversalschwingung des prismatischen Stabes*, ZAMM - Journal of Applied Mathematics and Mechanics / Zeitschrift für Angewandte Mathematik und Mechanik **15** (1935), 245.

[7] P. Schneider, R. Kienzler, (2011). *An Algorithm for the Automatisation of Pseudo Reductions of PDE Systems Arising from the Uniform-approximation Technique*, In: Shell-like Structures, H. Altenbach, V. Eremeyev (eds.), Advanced Structured Materials, Springer Berlin, Heidelberg (2011), 377–390.

[8] P. Schneider, R. Kienzler, *Comparison of various linear plate theories in the light of a consistent second-order approximation*, Mathematics and Mechanics of Solids (2014).

[9] P. Schneider, R. Kienzler, (2015). *On exact rod/beam/shaft-theories and the coupling among them due to arbitrary material anisotropies*, International Journal of Solids and Structures **56−57** (2015), 265–279.

[10] P. Schneider, *On the mathematical justification of the consistent-approximation approach and the derivation of a shear-correction-factor free refined beam theory*, Dissertation, Universität Bremen (2015).

[11] P. Schneider, R. Kienzler, M. Böhm, *Modeling of consistent second-order plate theories for anisotropic materials*, ZAMM - Journal of Applied Mathematics and Mechanics / Zeitschrift für Angewandte Mathematik und Mechanik **94**(1-2) (2014), 21–42.

Interfacial Phenomena in Materials: grain boundary kinematics and mechanics

David J Srolovitz

(joint work with Jian Han, Vaclav Vitek, Siu Sin Quek, YongWei Zhang)

Grain boundaries (GBs) exhibit many phenomena that impact mechanical properties. They are barriers to dislocation motion, they slide, they migrate in response to capillarity and applied stress, they absorb, emit, and transmit dislocations. This work provides an integrated picture of many of these properties based upon consideration of bicrystallography and the dislocations that it admits at interfaces. Some such dislocation are characterized by a Burgers vector and step and can glide along the grain boundary, giving rise to shear coupling (e.g., see [1, 2]. Simple statistical mechanics considerations show how shear coupling can change to GB sliding with increasing temperature. The same picture is applied to GB roughening. We show how these considerations (dislocation and step motion) can be used to describe GB migration driven by GB mean curvature. This same picture is used to describe how lattice dislocations entering the GB can decompose (get absorbed) and how such decomposition modifies and translates the GB structure and its local misorientation and inclination. This approach is extended to discuss the impact of GB migration on crystal lattice rotation and the plastic deformation of the grains bounding the GB.

The starting point of the analysis is bicrystallography as described in terms of the Coincident Site Lattice (CSL) and the Displacement Shift Complete (DSC) lattice [3], which describes the symmetry of crystallography of the **two** lattices that meet at the GB. The translation vectors of the DSC lattice describe all of the possible dislocation Burgers vectors $\mathbf{b}_{dsc}$. The shortest such $\mathbf{b}_{dsc}$s are small compared with the Burgers vectors $\mathbf{b}$ associated with the crystal lattices. Choose a GB plane that contains a periodic set of coincident lattice sites with normal $\mathbf{n}$. The DSC dislocation can only lie in the GB plane (the lattice Burgers vector, which is also a DSC Burgers vector, can also lie in the GB plane). For the case of $\mathbf{b}_{dsc} \cdot \mathbf{n} = 0$, the DSC dislocation also creates a step in the GB that translates the GB on one side of the DSC dislocation by a height h in the direction normal to the GB plane. The combination of the step and $\mathbf{b}_{dsc}$ is also known as a disconnection (e.g., see [5]. The glide of this disconnection along the GB translates one crystal with respect to the other (parallel to the GB plane) and translates the GB in the direction normal to the GB plane. The ratio of the parallel to perpendicular velocities is $\beta = v_{||}/v_n = \mathbf{b}_{dsc}/h$.

Each such $\mathbf{b}_{dsc}$, in fact, can have any one of a fixed set of step heights $h = j\lambda$, where j is any integer and λ is related to the reciprocal of the density of coincident sites, Σ [3]. Therefore, each GB does not have a unique value of β but in fact admits a set of values of β corresponding to the set of $\mathbf{b}_{dsc}$s parallel to the GB (there are a periodic set of these $\mathbf{b}_{dsc} = m\alpha$ where m is any integer and α is the shortest lattice spacing in the DSC lattice parallel to the GB plane) and the set of step heights for each; hence, $\beta = m/[m + j(\lambda/\alpha)]$ (N.B., this expression is not

general) [6, 7]. The question then arises: "which of these sets of $(\mathbf{b}_{dsc}, h)$ occur for a given GB?" Of course, crystallography cannot answer this question. Short of doing a full atomic scale simulation, we can assume a plausible form for the energy to insert a disconnection dipole on a GB: $\Delta E = 2\gamma|h| + 2E_{core} + (\mu b_{dsc}^2)/[4\pi(1-\nu)]\log(p/r_0) - p(\sigma\mathbf{n})\cdot\mathbf{b}_{dsc}$, where p is the spacing between steps, σ is the stress, E_{core} is the disconnection core energy, and γ is a constant that describes the energy per unit area of the step [8]. As the misorientation of the grains, grain boundary plane, magnitude and orientation of the applied stress changes, the set of σ and h that minimizes the energy will change. Given an energy function, a statistical mechanics approach was applied to predict the thermal average step height $< h(T) >$ and the grain boundary thickness $< h^2(T) >$. This approach has been shown to be consistent with the vast majority of atomistic simulation data for $\beta(T)$, GB roughness, and selection of (σ, h) as a function of GB misorientation and tilt axes [9].

$\mathbf{b}_{dsc}$s perpendicular to the GB can only move in the GB plane by absorption and emission of atoms (vacancies). For a general $\mathbf{b}_{dsc}$, any DSC dislocation can be written in terms of a combination of others that have $\mathbf{b}_{dsc}$s purely parallel or perpendicular to the GB plane. However, if these have large magnitudes, such decompositions may be too energetic to occur and hence the original $\mathbf{b}_{dsc}$ will not be able to glide without diffusion. This same approach can be used to understand the effectiveness of different grain boundaries as sources and sinks of point defects.

The Burgers vector of a lattice dislocation gliding into a CSL GB can be decomposed into DSC dislocations in the GB plane. The $\mathbf{b}_{dsc}\cdot\mathbf{n} = 0$ DSC dislocations can glide away with the normal component, however, cannot glide easily. Such components can be relaxed by emission of dislocations into the adjoining grain, yielding dislocation transmission. Such transmission events necessarily change the structure of the GB.

An open challenge is the description of GB migration in the language of disconnections. A few comments are in order. First, the curvature of a GB is proportional to the gradient in the step/disconnection density along the GB; this provides insight into the motion of GBs by mean curvature flow (especially if we include interactions between disconnections). Second, given the spatial distribution of $\mathbf{b}_{dsc}$s along a GB, $\rho_{b_i}(x)$, the boundary shape is $h(x) = \sum_i (1/\beta_i) \int_{-\infty}^{x} \rho_{b_i}(x')dx'$. This expression was confirmed by atomistic [10] and dislocation dynamics [11] simulation of the shear coupled migration of a GB bounded by a pair of GB triple junctions (lines along which the disconnections cannot glide).

While shear coupling can readily occur in the case of GBs in bicrystals, in polycrystalline materials, it is not possible to infinitely shear a grain in a polycrystal. As discussed above, GB (triple) junctions block the continued propagation of disconnections through the microstructure. Consider first the ideal case of a cylindrical grain of radius R completely embedded in another grain [1]. GB migration via mean curvature flow suggests $v_n = M\gamma\kappa = M\gamma/R$ (M and γ are the GB mobility and energy per unit area) and the shear velocity is $v_{||} = R\dot{\theta}$ (where $\dot{\theta}$ is the rotation rate of the cylindrical grain); the ratio of these two quantities is simply

the shear coupling β. Now, consider curvature-driven GB migration/rotation of a grain in a polycrystal where each grain has sharp corners (is not a cylinder). In this case, the rotation prescribed by β cannot continue because of these corners - stress must build up at these corners. The grain can respond in one of several ways: i) the growth in the elastic strain energy can compensate for the reduction in GB energy such that GB migration stops, ii) long range diffusion can occur on the length scale of the grain size (this is creep), iii) the GB migration can switch to a sliding mode (if the temperature is sufficiently large), or iv) the stress can lead to plasticity in the grain/emission and propagation of dislocations or twins that propagate across the grain [12]. All of these possible mechanism provide coupling between GB migration and other effects; elastic fields, diffusion, or crystal plasticity.

The results discussed here imply that GB migration necessarily implies the necessity of coupling of microstructure evolution and deformation in descriptions of both, the description of microstructure evolution within a finite deformation formalism, the importance of bicrystallography, and the possibility of describing microstructure evolution within a dislocation dynamics framework.

References

[1] J.W. Cahn, J.E. Taylor, *A unified approach to motion of grain boundaries, relative tangential translation along grain boundaries, and grain rotation*, Acta Mater. **52** (2004), 4887–4898.

[2] J.W. Cahn, Y. Mishin, A. Suzuki, *Coupling grain boundary motion to shear deformation*, Acta Mater. **54** (2006), 4953–4975.

[3] A. P. Sutton, R. W. Balluffi, *Interfaces in Crystalline Materials*, Oxford University Press, 1995.

[4] R.C. Pond, W. Bollmann, *The symmetry and interfacial structure of bicrystals*, Phil. Trans. R. Soc. Lond. A **292** (1979), 449–472.

[5] J.P. Hirth, R.C. Pond, *Steps, dislocations and disconnections as interface defects relating to structure and phase transformations*, Acta Mater. **44** (1996), 4749–4763.

[6] R.C. Pond, *Periodic Grain Boundary Structures in Aluminum*, Proc. R. Soc. A **357** (1977), 471–483.

[7] A.H. King, D.A. Smith, *The effects on grain-boundary processes of the steps in the boundary plane associated with the cores of grain-boundary dislocations*, Acta Crystallogr. A **36** (1980), 335–343.

[8] H. A. Khater, A. Serra, R.C. Pond, J.P.Hirth, *The disconnection mechanism of coupled migration and shear at grain boundaries*, Acta Mater. **60** (2012), 2007–2020.

[9] J. Han, V. Vitek, D.J. Srolovitz, to be published (2016).

[10] M. Aramfard, C. Deng, *Influences of triple junctions on stress-assisted grain boundary motion in nanocrystalline materials*, Modell. Simul. Mater. Sci. Eng. **22** (2014), 055012.

[11] S.S. Quek, Y.W. Zhang, D.J. Srolovitz, to be published (2016).

[12] M. Upmanyu, D.J. Srolovitz, A.E. Lobkovsky, J.A. Warren, W.C. Carter, *Simultaneous grain boundary migration and grain rotation*, Acta Mater. **54** (2006), 1707–1719.

On Generalized Interfaces. Kinematics, Balances and Damage. Coherent and Non-Coherent Cases

PAUL STEINMANN

(joint work with Ali Javeli, Ali Esmaeili)

The importance of interfaces is particularly appreciated at small length scales where they play a dominant role in the overall response of a body due to the large area to volume ratio [1]. Thereby, in general, coherent and non-coherent cases may be distinguished [2]. In the coherent case size effects can be captured by endowing the interface with its own kinematics, balances and constitutive behavior as proposed, e.g., by the interface elasticity theory. Interface elasticity theory proved already to be an extremely powerful tool to model size effects and the behavior of materials at very small length scales. However, to date, interface elasticity theory merely accounts for the elastic response of coherent interfaces and obviously fails to account for inelastic behavior such as damage. One aim of this contribution is thus to firstly extend interface elasticity theory to account for damage along coherent interfaces, i.e. in tangential direction to the coherent interface. The second objective of this contribution is then to further extend this approach to the non-coherent case by allowing for additional damage across non-coherent interfaces, i.e. in normal direction to the non-coherent interface. To this end, a thermodynamically consistent theory of generalized interfaces embracing both the coherent and the non-coherent case including damage along and across generalized interfaces is proposed. The degradation of the interface's mid-plane, i.e. the damage along the interface, is captured by a non-local damage model of integral-type. The out-of-plane de-cohesion, i.e. the damage across the interface, is described by a classical cohesive zone model. These models are then coupled through their corresponding damage variables. Based on the non-linear governing equations and the weak forms thereof the numerical implementation is carried out using the finite element method [3]. Finally, a series of numerical examples is studied to provide further insight into the coherent and the non-coherent cases and to carefully elucidate key features of the proposed theory.

REFERENCES

[1] A. Javeli, A. McBride, P. Steinmann, *Thermomechanics of Solids with Lower-Dimenisonal Energetics: On the Importance of Surface, Interface, and Curve Structures at the Nanoscale. A Unifying Review*, Applied Mechanics Reviews **65** (2013), 0802.

[2] A. Javeli, S. Kaessmair, P. Steinmann, *General Imperfect Interfaces*, Computer Methods in Applied Mechanics and Engineering **275** (2014), 76–97.

[3] A. Javeli, A. McBride, P. Steinmann, B.D. Reddy, *A Unified Computational Framework for Bulk and Surface Elasticity Theory: A Curvilinear-Coordinate-Based Finite Element Methodology*, Computational Mechanics **54** (2014), 745–762.

Atomistic & geometrically exact phase field modeling of nanoscopic dislocation processes

BOB SVENDSEN

(joint work with Jaber Rezeai Mianroodi)

The purpose of the current work is the development of a geometrically exact phase field model for dislocation dissociation, slip and stacking fault formation in single crystals amenable to determination via atomistic or *ab initio* methods in the spirit of computational material design. The current approach is based in particular on periodic microelasticity [4] to model the strongly non-local elastic interaction of dislocation lines via their (residual) strain fields. These strain fields depend in turn on phase fields which are used to parameterize the energy stored in dislocation lines and stacking faults. This energy storage is modeled here with the help of the "interface" energy concept and model of [1, 2, 6]. In particular, the "homogeneous" part of this energy is related to the "rigid" (i.e., purely translational) part of the displacement of atoms across the slip plane, while the "gradient" part accounts for energy storage in those regions near the slip plane where atomic displacements deviate from being rigid, e.g., in the dislocation core. Via the attendant global energy scaling, the interface energy model facilitates an atomistic determination of the entire phase field energy as an optimal approximation of the (exact) atomistic energy; no adjustable parameters remain. For simplicity, an interatomic potential and molecular statics are employed for this purpose here; alternatively, *ab initio* (i.e., DFT-based) methods can be used.

The current model formulation is compared with related models such as (generalized) Peierls-Nabarro [3] and phase field dislocation dynamics [5] models in the framework of classic density functional theory. The modeling of long-range dislocations interactions is shown to be equivalent in all of these; in constrast, that of the stacking fault and core energies differ. To investigate the consequences of different modeling assumptions, predictions from the models of [5] and [6] are compared with results from molecular statics (MS).

REFERENCES

[1] J. W. Cahn, J. E. Hilliard, *Free energy of a non-uniform system. I. Interfacial energy.*, Journal of Chemical Physics **28** (1958), 258-267–140.

[2] C. Shen, Y. Wang, *Incorporation of gamma-surface to phase field model of dislocations: simulation dislocation dissociation in fcc crystals* Acta Materialia **52** (2004), 683–691.

[3] Y. Xiang, H. Wei, P. Ming, W. E *A generalized Peirls-Nabarro model for curved dislocations and core structures of dislocation loops in Al and Cu*, Acta Materialia **56** (2008), 1447–1460.

[4] Y. Wang, J. Li, *Phase field modeling of defects and deformation*, Acta Materialia **58** (2010), 1212–1235.

[5] A. Hunter, I. J. Beyerlein, T. C. Germann, M. Koslowski, *Influence of the stacking fault energy surface on partial dislocations in fcc metals with a three dimensional phase field dynamics model*, Physical Review B **84** (2011), 144108.

[6] J. R. Mianroodi, B. Svendsen, *Atomistically determined phase field modeling of dislocation dissociation, stacking fault formation, dislocation slip, and reactions in fcc systems*, Journal of the Mechanics and Physics of Solids **77** (2015), 190–122.

Phase Field Method from a Physical Metallurgy Perspective
Yunzhi Wang

The phase field methods in modeling microstructural evolution during phase transformations and plastic deformation in solids are reviewed. As a continuum field theory of defects (i.e. microstructures) (similar to the density functional theory for electrons), the methods can be applied at both the fundamental defect level (from angstroms to nanometers) and coarse-grained level (from nanometers to microns) [1]. The gradient term in the phase field free energy functional appears naturally at the limit transitions of their counterpart discrete lattice models. When applied at the individual defect level the microscopic phase field model (MPF) is a super-set of the Cahn-Hilliard description of chemical inhomogeneities and the Peierls (cohesive zone) description of displacive inhomogeneities and it has the ability to predict fundamental properties of individual defects such as size, formation energy, saddle point configuration and activation energy of defect nuclei, and the micromechanisms of their mutual interactions, directly using ab initio calculations as model inputs. It is in particular good for the following applications:

- Using DFT calculations of generalized stacking fault (GSF) energy and multi-plane GSF and Landau free energy as direct inputs and predict defect structure, chemistry and energy.
- Probe the total energy landscape using nudged-elastic-band (NEB) method for saddle point configuration and activation energy of defect nucleation.
- When combined with experimental characterization, it could serve as a powerful tool to explore deformation/transformation mechanisms and provide critical inputs to coarse-grained phase field and crystal plasticity (CP) - FEM simulations.

Examples presented include (a) shape and activation energy of a critical nucleus during both homogeneous and heterogeneous transformations [1], [2], (b) structure and energy of a small angle twist grain boundary in Al and Cu [1], [3] and (c) detailed mechanisms of dislocation shearing of ordered intermetallic phases and formation of various stacking fault ribbons [4]–[7]. When applied at the mesoscopic level the coarse grained phase field model (CGPFM) has the ability to predict the evolution of microstructures consisting of a large assembly of both chemically and mechanically interacting defects through coupled displacive and diffusional mechanisms, with user-supplied linear response rate laws, defect energies and mobilities. It is in particular good for the following applications:

- Parametric study of collective behaviors of large defect ensemble with spatial correlation, interaction and co-evolution.
- Generate 3D synthetic microstructural datasets and repair experimental datasets and quantify SEM/TEM images for data analytics.
- Confirmation and realization of new ideas.

Examples presented include (a) dislocation-guided precipitation and formation of mesocrystlas [8], [9] and (b) variant selection during beta to alpha transformation in polycrystalline Ti-6Al-4V under different stress states [9], [10]. Integration of phase field techniques at different length scales (MPF and CGPFM) and integration of PFM with FFT-based crystal plasticity model to predict collective behavior of different population of defects including their mutual interactions and co-evolution holds great promise in modeling phase transformation and deformation with complex microstructural and chemical interactions. This has been demonstrated in modeling microstructural evolution during creep deformation of Ni-base superalloys [11], where precipitate microstructure and dislocation substructures co-evolve leading to rafting, and microstructure evolution during dynamic recrystallization of Cu [12], where grain structure and dislocation density co-evolve leading to stress redistribution and macroscopic softening.

REFERENCES

[1] Y. Wang, J. Li, *Acta Materialia Overview 150: Phase Field Modeling of Defects and Deformation*, Acta Mater. **58** (2010), 1212–1235.

[2] C. Shen, J. Li, Y. Wang, *Finding Critical Nucleus in Solid State Phase Transformations*, Met. Mater. Trans. A **39A** (2008), 976–983.

[3] C. Shen, J. Li, Y. Wang, *Predicting Structure and Energy of Dislocation and Grain Boundary*, Acta Mater. **74** (2014), 125–131.

[4] D. McAllister, D.C. Lv, B. Peterson, H. Deutchman, Y. Wang, M.J. Mills, *Lower Temperature Deformation Mechanisms in a gamma- Strengthened Ni-Base Superalloy*, Scripta Mater. **115** (2016), 108–112.

[5] N. Zhou, C. Shen, M.J. Mills, J. Li, Y. Wang, *Modeling Displacive-Diffusinal Coupled Dislocation Shearing of gamma Precipitates in Ni-Base Superalloys*, Acta Mater. **59** (2011), 3484–3497.

[6] R.R. Unocic, N. Zhou, L. Kovarik, C. Shen, Y. Wang, M.J. Mills, *Evolution of Deformation Microtwins during Creep of a gamma Precipitate Strengthened Ni-Base Superalloy*, Acta Mater. **59** (2011), 7325–7339.

[7] L. Kovarik, R.R. Unocic, J. Li, P. Sarosi, C. Shen, Y. Wang, M.J. Mills, *Microtwinning and Other Shearing Mechanisms at Intermediate Temperatures in Ni-Base Superalloys*, Prog. Mater. Sci. **54** (2009), 839–873.

[8] D. Qiu, R. Shi, D. Zhang, W. Lu, Y. Wang, *Variant selection by dislocations during alpha precipitation in alpha/beta titanium alloys*, Acta Mater. **88** (2015), 218–231.

[9] H. Liu, Y. Gao, Z. Xu, Y.M. Zhu, Y. Wang, J.F. Nie, *Guided Self-Assembly of Nano-Precipitates into Mesocrystals*, Scientific Report **5** (2015), 16530.

[10] R. Shi, N. Zhou, S. Niezgoda, Y. Wang, *Microstructure and Transformation Texture Evolution during α Precipitation in Polycrystalline alpha/beta Titanium Alloys - A Simulation Study*, Acta Mater. **94** (2015), 224–243.

[11] N. Zhou, C. Shen, M.J. Mills, Y. Wang, *Large-Scale Three-Dimensional Phase Field Simulation of gamma Rafting and Creep Deformation*, Phil. Mag. **90** (2010), 405–436.

[12] P.Y. Zhao, T.S.E. Low, Y. Wang, S.R. Niezgoda, *An integrated full-field modeling of concurrent plastic deformation and microstructure evolution: Application to 3D simulation of dynamic recrystallization in polycrystalline copper*, Int. J. Plasticity **80** (2016), 38–55.

25,000 Interface Simulations

DEREK WARNER

It is well known that grain boundaries can significantly influence the mechanical behavior of polycrystalline materials. This point has motivated a long-standing effort to better understand the behavior of grain boundaries, with a technological aim of (1) better predicting the deformation and failure of materials and (2) illuminating novel routes for creating improved materials via grain boundary engineering.

An important task in the quest to achieve these two goals is to establish a relationship between the geometry and mechanical properties of boundaries. Establishing such a relationship would enable qualitative assessment of the relative performance of materials given microstructure crystallographic data, some of which can be measured using electron backscatter diffraction technologies. Further, more quantitative predictions of material behavior using polycrystal physics-based microstructural models will benefit from an ability to link grain boundary geometry to properties, as there is currently no rational means of comprehensively assigning grain boundary properties in microstructural models. Describing the relationship between grain boundary geometry and mechanical properties is a longstanding challenge due to the complexity of the relationship and the vast geometric space in which grain boundaries reside. Previous efforts have examined the connection between grain boundary properties and simplified descriptors of boundary geometry, such as coincident site lattice (CSL) density, boundary energy, and boundary free volume. While these efforts have revealed that some rough trends do exist, the trends are not inclusive.

Following this motivation, results of a computational survey of the shear strength of a large set of grain boundaries are reported. The survey examined the shear strength as a function of shear direction for 343 unique grain boundary structures, making this study the most extensive of its kind to the author's knowledge. Results showed (1) no comprehensive relationships between grain boundary shear strength and eight common grain boundary descriptors, (2) a significant and simply describable dependence of shear strength on shear direction, and (3) that the grain boundary shear strengths in an ordinary polycrystalline material can be represented by a simple statistical distribution.

Shearband-based Computational Homogenization of Elastoplastic Microstructures With Hard Inclusions

STEPHAN WULFINGHOFF

(joint work with Stefanie Reese)

In this work, an efficient nonlinear homogenization method for geometrically simple microstructures is presented based on shear bands, that are activated in the microstructure. The degrees of freedom are strongly limited in comparison with full finite element method simulations.

Materials with inclusions and elastoplastic matrix often have favorable mechanical properties at a small density, which makes them attractive for a large range of applications. For linear materials, analytical homogenization methods often provide sufficiently accurate predictions. However, the non-linear case usually requires more advanced computational homogenization methods, like the FE^2-method [1]. Size-effects make matters usually even more complex [2, 3, 4]. Computational non-linear homogenization is usually associated with an increased computational effort. Here, a model that has been proposed in a recent work [5], is discussed. It represents an efficient homogenization method for physically non-linear elastoplastic microstructures with hard elastic inclusions and a soft inelastic, nearly incompressible matrix. An often seen mechanism in this kind of microstructure are shear bands with preferred directions. A conventional Ritz-Galerkin discretization is applied, i.e., the displacement is approximated by

$$(1) \qquad \mathbf{u}(\mathbf{x}, t) = \boldsymbol{\varepsilon}_0(t)\mathbf{x} + \sum_{i=1}^{N} \gamma_i^{\mathrm{s}}(t)\boldsymbol{\phi}_i^{\mathrm{s}}(\mathbf{x}).$$

Here, $\mathbf{u}(\mathbf{x}, t)$ is the displacement field and the $\boldsymbol{\phi}_i^{\mathrm{s}}(\mathbf{x})$ represent N ansatz functions. Moreover, γ_i^{s} are the degrees of freedom of the model. The shape functions $\boldsymbol{\phi}_i^{\mathrm{s}}(\mathbf{x})$ represent shear modes, which are defined on N shear bands. The same approximation as in [5] is applied. As a result, the strain reads

$$(2) \qquad \boldsymbol{\varepsilon} = sym\nabla\mathbf{u} = \boldsymbol{\varepsilon}_0 + \sum_{i} I_i(\mathbf{x})\gamma_i^{\mathrm{s}}\mathbf{M}_i^{\mathrm{s}}.$$

Here, $\mathbf{M}_i^{\mathrm{s}} = sym\mathbf{d}_i \otimes \mathbf{n}_i$ denote shear strain modes. The vectors $\mathbf{d}_i$ and $\mathbf{n}_i$ are unit vectors in the direction of the shear band and perpendicular, respectively. In Eq. (2), the function $I_i(\mathbf{x})$ represents the usual indicator function. The strain tensor $\boldsymbol{\varepsilon}_0$ can be shown to be given by

$$(3) \qquad \boldsymbol{\varepsilon}_0 = \boldsymbol{\varepsilon}_0(\bar{\boldsymbol{\varepsilon}}, \hat{\gamma}) = \bar{\boldsymbol{\varepsilon}} - \sum_{i} c_i\gamma_i^{\mathrm{s}}\mathbf{M}_i^{\mathrm{s}}$$

with $\hat{\gamma} = (\gamma_1^{\mathrm{s}}, \ldots, \gamma_N^{\mathrm{s}})$ and the shear band volume fraction c_i.
Assuming a quasi-static situation and neglecting body forces the equilibrium conditions can be given in weak form by

$$(4) \qquad \int_{\Omega} \boldsymbol{\sigma} \cdot \delta\boldsymbol{\varepsilon}d\Omega = 0.$$

Insertion of the ansatz then allows for the identification of N scalar nonlinear equations, which are solved via the standard Newton scheme.
In order to improve the accuracy of the method, [5] discussed several modifications of the method, which are beyond the scope of this work.

References

[1] F. Feyel, *Multiscale fe^2 elastoviscoplastic analysis of composite structures*, Computational Materials Science **16** (1999), 344–354.
[2] S. Wulfinghoff, E. Bayerschen, T. Böhlke *A gradient plasticity grain boundary yield theory*, International Journal of Plasticity **51** (2013), 33–46.

[3] S. Wulfinghoff, T. Böhlke, *Gradient crystal plasticity including dislocation-based work-hardening and dislocation transport*, International Journal of Plasticity **69** (2015), 152–169.

[4] S. Wulfinghoff, S. Forest, T. Böhlke, *Strain gradient plasticity modeling of the cyclic behavior of laminate microstructures*, Journal of the Mechanics and Physics of Solids **79** (2015), 1–20.

[5] S. Wulfinghoff, S. Reese, *Efficient computational homogenization of simple elastoplastic microstructures using a shear band approach*, Computer Methods in Applied Mechanics and Engineering **298** (2016), 350–372.

Design of Interfaces in Ceramic/Metallic Materials for High Energy Environments

Hussein Zbib

(joint work with George Ayoub, Wei Yang, Iman Salehinia and Mohsen Damadam)

Interfaces in metals, ceramics and alloys play a decisive role in determining the thermo-mechanical behavior under extreme loading and environmental conditions. To rationally design and accelerate discoveries of new material systems with novel thermo-mechanical properties-be it high temperature strength, corrosion resistance, fatigue life or any other mechanical property- the ability to predict the macroscopic properties on the basis of microstructure and interface structure is needed. The purpose of our work is to address this need by designing an engineered type of metal/ceramic nanocomposites with engineered nanolaminate structures that can exhibit very high strengths, fracture and fatigue resistance, thermal stability and corrosion resistance under high environment. Although refractory ceramic materials such as NbC and TiC, have high temperature strength and resistance to thermal shock and damage from thermal cycling, they are relatively brittle material with limited ductility and strength. However, laminate structures made of nanolayers with high density of incoherent interfaces (e.g. Nb on NbC and TiN on Ti), can have superior mechanical properties with strong resistance to thermal and environmental damage.

The metal/ceramic composites can be created layer by layer by gas phase atomic layer deposition which is useful for high aspect ratio and large area system in short times. An electrochemistry deposition may be used as well for many combinations of composites and layer thickness and morphology by changing the growth temperature, with the aim of optimizing thermo-mechanical properties. In our work, we employ a novel computational material-by-design approach that includes a multiscale computational framework bridging molecular and dislocation dynamics (microscale) with crystal plasticity (mesoscale) to (a) design composites with nanolaminates that can serve as the fundamental basis for metal/ceramic systems, and (b) study the thermo-mechanical properties, deformation, fracture and fatigue and corrosion resistance of a number of possible combinations of these nanocomposites.

Particularly, the characteristics of the interface structure and the deformation behavior of both nanoscale Ti-TiN and Nb-NbC multilayers with semi-coherent

interfaces were studied using MD simulations. The effect of temperature was also explored. Some key points are summarized as follows:

(1) The mechanisms of the formation of the interface misfit dislocation network iare characterized using AIFB theory that is the combination of MD simulation with the Frank-Bilby theory. Three sets of pure edge misfit dislocations and their Burgers vector are identified. Upon relaxation, stable T1 regions occupy large interface area. The higher energy stackings are transformed into misfit dislocations or dislocation nodes upon relaxation.

(2) The MD simulations show that plastic deformation in Ti/TiN multilayers commences first in the interface dislocation network. Shear stresses are generated around misfit lines and push the dislocations in the coherent regions in the interface, resulting in the 1st yield in the stress-strain curve. The material is strain hardened upon further compression until the stress is enough to nucleate dislocations on the pyramidal slip planes in Ti. The 2nd major yield point occurs due to dislocation nucleation in the Ti layer. Strain hardening continues after the 2nd yield point due to the dislocations deposition in the interface and dislocations interactions in the Ti layer. The 3rd major yield occurs when dislocations nucleate/transfer into the TiN layer. At this point Ti and TiN layers co-deform plastically and no visible crack is observed.

(3) The stress-strain curves show the same trends possessing three distinct yield points at various temperatures. However, the stresses at the yield points drop at higher temperatures.

(4) The bilayer structure of Nb/NbC was studied under different types of loadings: uniaxial tension, uniaxial compression and, biaxial loading. The results show that dislocations nucleate in the Nb layer while there is no evidence of plastic deformation in the ceramic layer. By examining the resulting stress-strain curves, the state of stress to initiate plastic deformation (yield stress in tension/compression) is identified and the yield surface for Nb/NbC is determined under different combinations of biaxial tensile and compressive loadings. The result can be used to establish plastic flow potential for use in continuum theory for large-scale applications.

Low volume-fraction microstructures in shape memory alloys

Barbara Zwicknagl

(joint work with Sergio Conti and Johannes Diermeier)

We discuss recent analytical results on microstructures near austenite-martensite interfaces in shape memory alloys with almost compatible phases. Such materials have gained growing attention in the last decade since compatibility appears to be related to particularly low hysteresis and high reversibility of the phase transition (see e.g. [4, 9]). To better understand the energy barrier leading to hysteresis and the associated microstructures, we study a variational problem that has been introduced to describe microstructures near austenite-martensite interfaces (see

[7, 8]). Precisely, we minimize functionals of the form

$$J_\theta(u) := \mu \int_0^\infty \int_0^1 |\nabla u|^2 + \int_{-L}^0 \int_0^1 \text{dist}^2(\nabla u, K_\theta) + \varepsilon \int_{-L}^0 \int_0^1 |\partial_y \partial_y u|.$$

The first term stands for the elastic energy of austenite, the second term for the elastic energy of martensite, where $K_\theta = \{(0, \theta)^T, (0, -1 + \theta)^T\}$ represents two martensitic wells, and the last term, to be understood distributionally, is a regularization term which can be interpreted as a surface energy. Here, $\theta \in (0, 1/2]$ measures the compatibility of the phases, the parameter μ represents the ratio between the elastic moduli of austenite and martensite, and ε stands for a typical surface energy constant per unit length.

Rigid austenite. In the case of relatively rigid austenite, we find the following scaling behavior of the minimal energy (see [10, Theorem 1], which is based on [8, 1], see also [5]): There is a constant $c > 0$ such that for all $\mu \geq 1$, all $\varepsilon > 0$, and all $\theta \in (0, 1/2]$, we have, with $\hat{\varepsilon} := \varepsilon/\theta^2$,

$$\frac{1}{c} \min\{\hat{\varepsilon}^{2/3} L^{1/3}, \hat{\varepsilon}^{1/2}, 1, L\} \leq \min J_\theta(u)/\theta^2 \leq c \min\{\hat{\varepsilon}^{2/3} L^{1/3}, \hat{\varepsilon}^{1/2}, 1, L\}.$$

The first two scaling regimes correspond to branched patterns, the remaining two ones to uniform structures, i.e., to constant, respectively affine functions in the martensite bulk. To better understand the transition from uniform structures to complex patterns we investigate in [2] (see also [6]) for $\mu = \infty$ and $L = 1$ the critical regime $\hat{\varepsilon} = const$ in the limit of almost compatible phases $\theta \to 0$. Then the minority phase concentrates on lines, and it turns out that the rescaled functionals $E_\theta(v) := J_\theta(\theta v)/\theta^2$ converge in the sense of Γ-convergence with respect to the L^1-topology to a functional of Mumford-Shah type where admissible functions $v \in SBV_{\text{loc}}$ satisfy additional constraints on their jump sets. The main difficulty lies in the proof of the upper bound, which requires a density result in the set of admissible functions.

Soft austenite. In the case of relatively soft austenite, the phase diagram turns out to be more complex. Restricting the class of admissible functions to $\mathcal{A} := \{u \in W_{\text{loc}}^{1,2}((-L, 0) \times (0, 1)) : \partial_y u \in \{\theta, -1 + \theta\} \text{ a.e. in } \{x < 0\}\}$, we are led to consider the model introduced in [7, 8], and we find the following scaling behavior (see [3, Theorem 1]): There is a constant $c > 0$ such that for all $\mu, L, \varepsilon > 0$, and all $\theta \in (0, 1/2]$, setting again $\hat{\varepsilon} := \varepsilon/\theta^2$,

$$\frac{1}{c} \min_{u \in \mathcal{A}} \frac{J_\theta(u)}{\theta^2} \leq \min \left\{ \hat{\varepsilon}^{2/3} L^{1/3}, \hat{\varepsilon}^{1/2}, (\hat{\varepsilon} L \mu)^{1/2} \ln^{1/2}\left(3 + \frac{\hat{\varepsilon}}{\mu^3 L}\right), \right.$$

$$\left. (\hat{\varepsilon} L \mu)^{1/2} \ln^{1/2}\left(\frac{1}{\theta}\right), \mu \right\} \leq c \min_{u \in \mathcal{A}} \frac{J_\theta(u)}{\theta^2}.$$

The case $\theta = 1/2$ has been studied in [8, 1], and the main new result here is the appearance of a new regime with scaling $(\hat{\varepsilon} L \mu)^{1/2} \ln^{1/2}\left(3 + \frac{\hat{\varepsilon}}{\mu^3 L}\right)$ which corresponds to a two-scale branching construction that lies in between laminates with scaling $(\hat{\varepsilon} L \mu)^{1/2} \ln^{1/2}\left(\frac{1}{\theta}\right)$ and branching with scaling $\hat{\varepsilon}^{2/3} L^{1/3}$.

References

[1] S. Conti, *A lower bound for a variational model for pattern formation in shape-memory alloys*, Cont. Mech. Thermodyn. **17**(6) (2006), 469–476.

[2] S. Conti, J. Diermeier, B. Zwicknagl, *Deformation concentration for martensitic microstructures in the limit of low volume fraction*, Preprint arXiv:1512.07023 (2015).

[3] S. Conti, B. Zwicknagl, *Low volume-fraction microstructures in martensites and crystal plasticity*, to appear in Math. Models Meth. Appl. Sci., DOI: 10.1142/S0218202516500317, see also arXiv:1507.04521 (2015).

[4] J. Cui, Y. Chu, O. Famodu, Y. Furuya, J. Hattrick-Simpers, R. James, A. Ludwig, S. Thienhaus, M. Wuttig, Z. Zhang, I. Takeuchi, *Combinatorial search of thermoelastic shape-memory alloys with extremely small hysteresis width*, Nature materials **5** (2006), 286–290.

[5] J. Diermeier, *Nichtkonvexe Variationsprobleme und Mikrostrukturen.* Bachelor's thesis, Universität Bonn (2010).

[6] J. Diermeier, *A low volume-fraction limit for martensitic microstructures in shape-memory alloys*, Proc. Appl. Math. Mech. **15** (2015), 541–542.

[7] R. Kohn, S. Müller, *Branching of twins near an austenite-twinned martensite interface*, Phil. Mag. A **66** (1992), 697–715.

[8] R. Kohn, S. Müller, *Surface energy and microstructure in coherent phase transitions*, Comm. Pure Appl. Math. **XLVII** (1994), 405–435.

[9] Z. Zhang, R.D. James, S. Müller, *Energy barriers and hysteresis in martensitic phase transformations*, Acta Materialia **57**(15) (2007), 4332–4352.

[10] B. Zwicknagl, *Microstructures in low-hysteresis shape memory alloys: Scaling regimes and optimal needle shapes*, Arch. Rat. Mech. Anal. **213** (2014), 355–421.

Reporter: Ewald A. Werner

Participants

Dr. B. Emek Abali
Institut für Mechanik, Sekr. MS 2
FG Kontinuumsmechanik &
Materialtheorie
Technische Universität Berlin
Einsteinufer 5
10587 Berlin
GERMANY

Prof. Dr. Amit Acharya
Dept. of Civil & Environmental
Engineering
Carnegie Mellon University
101 Porter Hall
Pittsburgh, PA 15213-3890
UNITED STATES

Prof. Dr. Holm Altenbach
Fakultät für Maschinenbau
Otto-von-Guericke-Universität
Magdeburg
39106 Magdeburg
GERMANY

Prof. Dr. Albrecht Bertram
Institut für Mechanik
Otto-von-Guericke-Universität
Magdeburg
39106 Magdeburg
GERMANY

Prof. Dr. Thomas Bieler
College of Engineering
Dept. of Materials Science &
Engineering
Michigan State University
Engineering Building
428 S. Shaw Lane
East Lansing, MI 48824-1226
UNITED STATES

Prof. Dr. Long-Qing Chen
Materials Science and Engineering
Pennsylvania State University
University Park, PA 16802
UNITED STATES

Prof. Dr. Youping Chen
Dept. of Mechanical & Aerospace
Engineering
University of Florida (228 MAE-B)
P.O. Box 116250
Gainesville, FL 32611
UNITED STATES

Prof. Dr. Michael J. Demkowicz
Department of Mathematics
Texas A & M University
College Station, TX 77843-3368
UNITED STATES

Lukas Döring
Lehrstuhl I für Mathematik
RWTH Aachen
Templergraben 55
52062 Aachen
GERMANY

Peter Gladbach
Institut für Angewandte Mathematik
Universität Bonn
Endenicher Allee 60
53115 Bonn
GERMANY

Dr. Rainer Glüge
Institut für Mechanik
Otto-von-Guericke-Universität
Magdeburg
39106 Magdeburg
GERMANY

Prof. Dr. Klaus Hackl
Lehrstuhl für Mechanik - Materialtheorie
Fak. für Bau- Umwelt- u.
Ingenieurwissenschaften
Ruhr-Universität Bochum
44801 Bochum
GERMANY

Prof. Dr. Thomas Hochrainer
Bremer Institut für Strukturmechanik
und Produktionsanlagen BIME
IW3
Am Biologischen Garten 2
28359 Bremen
GERMANY

Dr.-Ing. Jörn Ihlemann
Institut für Mechanik und
Thermodynamik
Technische Universität Chemnitz
Straße der Nationen 62
09111 Chemnitz
GERMANY

Prof. Dr. Richard D. James
Department of Aerospace Engineering
and Mechanics
University of Minnesota
110 Union Street S. E.
Minneapolis, MN 55455
UNITED STATES

Prof. Dr. Reinhold Kienzler
FB 4 / FG 15 / IW 3
Universität Bremen
Postfach 33 04 40
28334 Bremen
GERMANY

Prof. Dr. Dennis M. Kochmann
Graduate Aerospace Laboratories
CALTECH, MS 105-50
1200 East California Boulevard
Pasadena, CA 91125
UNITED STATES

Dr. Carolin Kreisbeck
Fakultät für Mathematik
Universität Regensburg
93053 Regensburg
GERMANY

Dr.-Ing. Christian Krempaszky
Lehrstuhl für Werkstoffkunde
und Werkstoffmechanik
Technische Universität München
Boltzmannstrasse 15
85747 Garching
GERMANY

Marat I. Latypov
Georgia Tech-Lorraine
GT - CNRS UMI 2958
2, Rue Marconi
57070 Metz
FRANCE

Prof. Dr. Khanh Chau Le
Lehrstuhl für Allgemeine Mechanik
Fakultät für Bauingenieurwesen
Ruhr-Universität Bochum
Universitätsstrasse 150
44801 Bochum
GERMANY

Prof. Dr. Robert Lipton
Department of Mathematics
Louisiana State University
Baton Rouge LA 70803-4918
UNITED STATES

Prof. Dr. David L. McDowell
The George W. Woodruff School of
Mechanical Engineering and
School of Materials Science and
Engineering
Georgia Institute of Technology
Atlanta, GA 30332-0405
UNITED STATES

Felix Meier
Lehrstuhl f. Werkstoffkunde &
Werkstoffmechanik
Technische Universität München
Boltzmannstrasse 15
85747 Garching
GERMANY

Prof. Dr. Sinisa Mesarovic
School of Mechanical & Materials
Engineering
Washington State University
Pullman, WA 99164-2920
UNITED STATES

Prof. Dr. Alexander Mielke
Weierstraß-Institut für Angewandte
Analysis und Stochastik
Mohrenstrasse 39
10117 Berlin
GERMANY

Prof. Dr. Stefan Müller
Hausdorff Center for Mathematics
Institute for Applied Mathematics
Endenicher Allee 60
53115 Bonn
GERMANY

Prof. Dr. Stefan Neukamm
Fachrichtung Mathematik
Technische Universität Dresden
01062 Dresden
GERMANY

Henning Pöttker
Institut für Angewandte Mathematik
Universität Bonn
53115 Bonn
GERMANY

Prof. Dr. Anja Schlömerkemper
Institut für Mathematik
Universität Würzburg
Emil-Fischer-Strasse 40
97074 Würzburg
GERMANY

Dr. Patrick Schneider
FB 4 / FG 15 / IW3
Universität Bremen
Postfach 33 04 40
28334 Bremen
GERMANY

Prof. Dr. Jörg Schröder
Institut für Mechanik
Universität Duisburg-Essen
45117 Essen
GERMANY

Prof. Dr. David J. Srolovitz
School of Engineering and Applied
Sciences
University of Pennsylvania
220 South 33rd Street
Philadelphia, PA 19194-6391
UNITED STATES

Prof. Dr. Paul Steinmann
Lehrstuhl für Technische Mechanik
Universität Erlangen
Postfach 3429
91022 Erlangen
GERMANY

Prof. Dr. Bob Svendsen
Material Mechanics
Jülich Aachen Research Alliance
RWTH Aachen
Schinkelstrasse 2
52062 Aachen
GERMANY

Prof. Dr. Yunzhi Wang
Materials Science and Engineering
The Ohio State University
2041 College Road
Columbus, OH 43210
UNITED STATES

Prof. Dr. Derek H. Warner
College of Engineering
Cornell University
Carpenter Hall
Ithaca, NY 14853-2201
UNITED STATES

Prof. Dr. Ewald A. Werner
Lehrstuhl f. Werkstoffkunde &
Werkstoffmechanik
Technische Universität München
Boltzmannstrasse 15
85747 Garching
GERMANY

Dr. Stephan Wulfinghoff
Institut für Angewandte Mechanik
RWTH Aachen
Mies-van-der-Rohe-Strasse 1
52074 Aachen
GERMANY

Prof. Dr. Hussein M. Zbib
School of Mechanical & Materials
Engineering
Washington State University
Pullman, WA 99164-2920
UNITED STATES

Prof. Dr. Ting Zhu
Woodruff School of Mechanical
Engineering
Georgia Institute of Technology
Atlanta, GA 30332
UNITED STATES

Dr. Barbara Zwicknagl
Institut für Angewandte Mathematik
Universität Bonn
Endenicher Allee 62
53115 Bonn
GERMANY